Title

A Search for IceCube Sub-TeV Neutrinos Correlated with Gravitational-wave Events Detected By LIGO/Virgo

Permalink

https://escholarship.org/uc/item/17p1277m

Journal

The Astrophysical Journal, 959(2)

ISSN

0004-637X

Authors

Abbasi, R
Ackermann, M
Adams, J
et al.

Publication Date

2023-12-01

DOI

10.3847/1538-4357/aceefc

Copyright Information

Peer reviewed

A Search for IceCube Sub-TeV Neutrinos Correlated with Gravitational-wave Events Detected By LIGO/Virgo

R. Abbasi[1], M. Ackermann[2], J. Adams[3], S. K. Agarwalla[4,65], J. A. Aguilar[5], M. Ahlers[6], J. M. Alameddine[7],
N. M. Amin[8], K. Andeen[9], G. Anton[10], C. Argüelles[11], Y. Ashida[4], S. Athanasiadou[2], S. N. Axani[8], X. Bai[12],
A. Balagopal V.[4], M. Baricevic[4], S. W. Barwick[13], V. Basu[4], R. Bay[14], J. J. Beatty[15,16], K.-H. Becker[17],
J. Becker Tjus[18,66], J. Beise[19], C. Bellenghi[20], S. BenZvi[21], D. Berley[22], E. Bernardini[23], D. Z. Besson[24],
G. Binder[14,25], D. Bindig[17], E. Blaufuss[22], S. Blot[2], F. Bontempo[26], J. Y. Book[11], C. Boscolo Meneguolo[23], S. Böser[27],
O. Botner[19], J. Böttcher[28], E. Bourbeau[6], J. Braun[4], B. Brinson[29], J. Brostean-Kaiser[2], R. T. Burley[30], R. S. Busse[31],
D. Butterfield[4], M. A. Campana[32], K. Carloni[11], E. G. Carnie-Bronca[30], S. Chattopadhyay[4,65], N. Chau[5], C. Chen[29],
Z. Chen[33], D. Chirkin[4], S. Choi[34], B. A. Clark[22], L. Classen[31], A. Coleman[19], G. H. Collin[35], A. Connolly[15,16],
J. M. Conrad[35], P. Coppin[36], P. Correa[36], S. Countryman[37], D. F. Cowen[38,39], P. Dave[29], C. De Clercq[36],
J. J. DeLaunay[40], D. Delgado López[11], H. Dembinski[8], K. Deoskar[41], A. Desai[4], P. Desiati[4], K. D. de Vries[36],
G. de Wasseige[42], T. DeYoung[43], A. Diaz[35], J. C. Díaz-Vélez[4], M. Dittmer[31], A. Domi[10], H. Dujmovic[4],
M. A. DuVernois[4], T. Ehrhardt[27], P. Eller[20], R. Engel[26,44], H. Erpenbeck[4], J. Evans[22], P. A. Evenson[8], K. L. Fan[22],
K. Fang[4], A. R. Fazely[45], A. Fedynitch[46], N. Feigl[47], S. Fiedlschuster[10], C. Finley[41], L. Fischer[2], D. Fox[38],
A. Franckowiak[18], E. Friedman[22], A. Fritz[27], P. Fürst[28], T. K. Gaisser[8], J. Gallagher[48], E. Ganster[28], A. Garcia[11],
L. Gerhardt[25], A. Ghadimi[40], C. Glaser[19], T. Glauch[20], T. Glüsenkamp[10,19], N. Goehlke[44], J. G. Gonzalez[8],
S. Goswami[40], D. Grant[43], S. J. Gray[22], S. Griffin[4], S. Griswold[21], C. Günther[28], P. Gutjahr[7], C. Haack[20],
A. Hallgren[19], R. Halliday[43], L. Halve[28], F. Halzen[4], H. Hamdaoui[33], M. Ha Minh[20], K. Hanson[4], J. Hardin[35],
A. A. Harnisch[43], P. Hatch[49], A. Haungs[26], K. Helbing[17], J. Hellrung[18], F. Henningsen[20], L. Heuermann[28], N. Heyer[19],
S. Hickford[17], A. Hidvegi[41], C. Hill[50], G. C. Hill[30], K. D. Hoffman[22], K. Hoshina[4,67], W. Hou[26], T. Huber[26],
K. Hultqvist[41], M. Hünnefeld[7], R. Hussain[4], K. Hymon[7], S. In[34], A. Ishihara[50], M. Jacquart[4], M. Jansson[41], G. S. Japaridze[51],
K. Jayakumar[4,65], M. Jeong[34], M. Jin[11], B. J. P. Jones[52], D. Kang[26], W. Kang[34], X. Kang[32], A. Kappes[31],
D. Kappesser[27], L. Kardum[7], T. Karg[2], M. Karl[20], A. Karle[4], U. Katz[10], M. Kauer[4], J. L. Kelley[4],
A. Khatee Zathul[4], A. Kheirandish[53,54], J. Kiryluk[33], S. R. Klein[14,25], A. Kochocki[43], R. Koirala[8], H. Kolanoski[47],
T. Kontrimas[20], L. Köpke[27], C. Kopper[43], D. J. Koskinen[6], P. Koundal[26], M. Kovacevich[32], M. Kowalski[2,47],
T. Kozynets[6], K. Kruiswijk[42], E. Krupczak[43], A. Kumar[2], E. Kun[18], N. Kurahashi[32], N. Lad[2], C. Lagunas Gualda[2],
M. Lamoureux[42], M. J. Larson[22], F. Lauber[17], J. P. Lazar[4,11], J. W. Lee[34], K. Leonard DeHolton[38,39],
A. Leszczyńska[8], M. Lincetto[18], Q. R. Liu[4], M. Liubarska[55], E. Lohfink[27], C. Love[32], C. J. Lozano Mariscal[31], L. Lu[4],
F. Lucarelli[56], A. Ludwig[57], W. Luszczak[15,16], Y. Lyu[14,25], J. Madsen[4], K. B. M. Mahn[43], Y. Makino[4], S. Mancina[4,23],
W. Marie Sainte[4], I. C. Mariş[5], S. Marka[37], Z. Marka[37], M. Marsee[40], I. Martinez-Soler[11], R. Maruyama[58], F. Mayhew[43],
T. McElroy[55], F. McNally[59], J. V. Mead[6], K. Meagher[4], S. Mechbal[2], A. Medina[16], M. Meier[50], S. Meighen-Berger[20],
Y. Merckx[36], L. Merten[18], J. Micallef[43], T. Montaruli[56], R. W. Moore[55], Y. Morii[50], R. Morse[4], M. Moulai[4],
T. Mukherjee[26], R. Naab[2], R. Nagai[50], M. Nakos[4], U. Naumann[17], J. Necker[2], M. Neumann[31], H. Niederhausen[43],
M. U. Nisa[43], A. Noell[28], S. C. Nowicki[43], A. Obertacke Pollmann[50], V. O'Dell[4], M. Oehler[26], B. Oeyen[60], A. Olivas[22],
R. Orsoe[20], J. Osborn[4], E. O'Sullivan[19], H. Pandya[8], N. Park[49], G. K. Parker[52], E. N. Paudel[8], L. Paul[9],
C. Pérez de los Heros[19], J. Peterson[4], S. Philippen[28], S. Pieper[17], A. Pizzuto[4], M. Plum[12], A. Pontén[19], Y. Popovych[27],
M. Prado Rodriguez[4], B. Pries[43], R. Procter-Murphy[22], G. T. Przybylski[25], J. Rack-Helleis[27], K. Rawlins[61], Z. Rechav[4],
A. Rehman[8], P. Reichherzer[18], G. Renzi[5], E. Resconi[20], S. Reusch[2], W. Rhode[7], M. Richman[32], B. Riedel[4],
E. J. Roberts[30], S. Robertson[14,25], S. Rodan[34], G. Roellinghoff[34], M. Rongen[27], C. Rott[34,62], T. Ruhe[7], L. Ruohan[20],
D. Ryckbosch[60], S. Athanasiadou[2], I. Safa[4,11], J. Saffer[44], D. Salazar-Gallegos[43], P. Sampathkumar[26],
S. E. Sanchez Herrera[43], A. Sandrock[7], M. Santander[40], S. Sarkar[55], S. Sarkar[63], J. Savelberg[28], P. Savina[4], M. Schaufel[28],
H. Schieler[26], S. Schindler[10], B. Schlüter[31], F. Schlüter[5], T. Schmidt[22], J. Schneider[10], F. G. Schröder[8,26],
L. Schumacher[20], G. Schwefer[28], S. Sclafani[32], D. Seckel[8], S. Seunarine[64], A. Sharma[19], S. Shefali[44], N. Shimizu[50],
M. Silva[4], B. Skrzypek[11], B. Smithers[52], R. Snihur[4], J. Soedingrekso[7], A. Søgaard[6], D. Soldin[44], G. Sommani[18],
C. Spannfellner[20], G. M. Spiczak[64], C. Spiering[2], M. Stamatikos[16], T. Stanev[8], T. Stezelberger[25], T. Stürwald[17],
T. Stuttard[6], G. W. Sullivan[22], I. Taboada[29], S. Ter-Antonyan[45], W. G. Thompson[11], J. Thwaites[4], S. Tilav[8],
K. Tollefson[43], C. Tönnis[34], S. Toscano[5], D. Tosi[4], A. Trettin[2], C. F. Tung[29], R. Turcotte[26], J. P. Twagirayezu[43], B. Ty[4],
M. A. Unland Elorrieta[31], A. K. Upadhyay[4,65], K. Upshaw[45], N. Valtonen-Mattila[19], J. Vandenbroucke[4],
N. van Eijndhoven[36], D. Vannerom[35], J. van Santen[2], J. Vara[31], J. Veitch-Michaelis[4], M. Venugopal[26], S. Verpoest[60],
D. Veske[37], C. Walck[41], T. B. Watson[52], C. Weaver[43], P. Weigel[35], A. Weindl[26], J. Weldert[38,39], C. Wendt[4],
J. Werthebach[7], M. Weyrauch[26], N. Whitehorn[43,57], C. H. Wiebusch[28], N. Willey[43], D. R. Williams[40], M. Wolf[20],
G. Wrede[10], X. W. Xu[45], J. P. Yanez[55], E. Yildizci[4], S. Yoshida[50], F. Yu[11], S. Yu[43], T. Yuan[4], Z. Zhang[33], and P. Zhelnin[11]

The IceCube Collaboration

[1] Department of Physics, Loyola University Chicago, Chicago, IL 60660, USA; analysis@icecube.wisc.edu
[2] Deutsches Elektronen-Synchrotron DESY, Platanenallee 6, D-15738 Zeuthen, Germany
[3] Dept. of Physics and Astronomy, University of Canterbury, Private Bag 4800, Christchurch, New Zealand
[4] Dept. of Physics and Wisconsin IceCube Particle Astrophysics Center, University of Wisconsin–Madison, Madison, WI 53706, USA
[5] Université Libre de Bruxelles, Science Faculty CP230, B-1050 Brussels, Belgium
[6] Niels Bohr Institute, University of Copenhagen, DK-2100 Copenhagen, Denmark
[7] Dept. of Physics, TU Dortmund University, D-44221 Dortmund, Germany
[8] Bartol Research Institute and Dept. of Physics and Astronomy, University of Delaware, Newark, DE 19716, USA
[9] Department of Physics, Marquette University, Milwaukee, WI 53201, USA
[10] Erlangen Centre for Astroparticle Physics, Friedrich-Alexander-Universität Erlangen-Nürnberg, D-91058 Erlangen, Germany
[11] Department of Physics and Laboratory for Particle Physics and Cosmology, Harvard University, Cambridge, MA 02138, USA
[12] Physics Department, South Dakota School of Mines and Technology, Rapid City, SD 57701, USA
[13] Dept. of Physics and Astronomy, University of California, Irvine, CA 92697, USA
[14] Dept. of Physics, University of California, Berkeley, CA 94720, USA
[15] Dept. of Astronomy, Ohio State University, Columbus, OH 43210, USA
[16] Dept. of Physics and Center for Cosmology and Astro-Particle Physics, Ohio State University, Columbus, OH 43210, USA
[17] Dept. of Physics, University of Wuppertal, D-42119 Wuppertal, Germany
[18] Fakultät für Physik & Astronomie, Ruhr-Universität Bochum, D-44780 Bochum, Germany
[19] Dept. of Physics and Astronomy, Uppsala University, Box 516, S-75120 Uppsala, Sweden
[20] Physik-department, Technische Universität München, D-85748 Garching, Germany
[21] Dept. of Physics and Astronomy, University of Rochester, Rochester, NY 14627, USA
[22] Dept. of Physics, University of Maryland, College Park, MD 20742, USA
[23] Dipartimento di Fisica e Astronomia Galileo Galilei, Università Degli Studi di Padova, I-35122 Padova PD, Italy
[24] Dept. of Physics and Astronomy, University of Kansas, Lawrence, KS 66045, USA
[25] Lawrence Berkeley National Laboratory, Berkeley, CA 94720, USA
[26] Karlsruhe Institute of Technology, Institute for Astroparticle Physics, D-76021 Karlsruhe, Germany
[27] Institute of Physics, University of Mainz, Staudinger Weg 7, D-55099 Mainz, Germany
[28] III. Physikalisches Institut, RWTH Aachen University, D-52056 Aachen, Germany
[29] School of Physics and Center for Relativistic Astrophysics, Georgia Institute of Technology, Atlanta, GA 30332, USA
[30] Department of Physics, University of Adelaide, Adelaide, 5005, Australia
[31] Institut für Kernphysik, Westfälische Wilhelms-Universität Münster, D-48149 Münster, Germany
[32] Dept. of Physics, Drexel University, 3141 Chestnut Street, Philadelphia, PA 19104, USA
[33] Dept. of Physics and Astronomy, Stony Brook University, Stony Brook, NY 11794-3800, USA
[34] Dept. of Physics, Sungkyunkwan University, Suwon 16419, Republic of Korea
[35] Dept. of Physics, Massachusetts Institute of Technology, Cambridge, MA 02139, USA
[36] Vrije Universiteit Brussel (VUB), Dienst ELEM, B-1050 Brussels, Belgium
[37] Columbia Astrophysics and Nevis Laboratories, Columbia University, New York, NY 10027, USA
[38] Dept. of Astronomy and Astrophysics, Pennsylvania State University, University Park, PA 16802, USA
[39] Dept. of Physics, Pennsylvania State University, University Park, PA 16802, USA
[40] Dept. of Physics and Astronomy, University of Alabama, Tuscaloosa, AL 35487, USA
[41] Oskar Klein Centre and Dept. of Physics, Stockholm University, SE-10691 Stockholm, Sweden
[42] Centre for Cosmology, Particle Physics and Phenomenology—CP3, Université catholique de Louvain, Louvain-la-Neuve, Belgium
[43] Dept. of Physics and Astronomy, Michigan State University, East Lansing, MI 48824, USA
[44] Karlsruhe Institute of Technology, Institute of Experimental Particle Physics, D-76021 Karlsruhe, Germany
[45] Dept. of Physics, Southern University, Baton Rouge, LA 70813, USA
[46] Institute of Physics, Academia Sinica, Taipei 11529, Taiwan
[47] Institut für Physik, Humboldt-Universität zu Berlin, D-12489 Berlin, Germany
[48] Dept. of Astronomy, University of Wisconsin–Madison, Madison, WI 53706, USA
[49] Dept. of Physics, Engineering Physics, and Astronomy, Queen's University, Kingston, ON K7L 3N6, Canada
[50] Dept. of Physics and The International Center for Hadron Astrophysics, Chiba University, Chiba 263-8522, Japan
[51] CTSPS, Clark-Atlanta University, Atlanta, GA 30314, USA
[52] Dept. of Physics, University of Texas at Arlington, 502 Yates Street, Science Hall Rm 108, Box 19059, Arlington, TX 76019, USA
[53] Department of Physics & Astronomy, University of Nevada, Las Vegas, NV 89154, USA
[54] Nevada Center for Astrophysics, University of Nevada, Las Vegas, NV 89154, USA
[55] Dept. of Physics, University of Alberta, Edmonton, Alberta T6G 2E1 Canada
[56] Département de physique nucléaire et corpusculaire, Université de Genève, CH-1211 Genève, Switzerland
[57] Department of Physics and Astronomy, UCLA, Los Angeles, CA 90095, USA
[58] Dept. of Physics, Yale University, New Haven, CT 06520, USA
[59] Department of Physics, Mercer University, Macon, GA 31207-0001, USA
[60] Dept. of Physics and Astronomy, University of Gent, B-9000 Gent, Belgium
[61] Dept. of Physics and Astronomy, University of Alaska Anchorage, 3211 Providence Drive, Anchorage, AK 99508, USA
[62] Department of Physics and Astronomy, University of Utah, Salt Lake City, UT 84112, USA

[63] Dept. of Physics, University of Oxford, Parks Road, Oxford OX1 3PU, UK
[64] Dept. of Physics, University of Wisconsin, River Falls, WI 54022, USA

Abstract

The LIGO/Virgo collaboration published the catalogs GWTC-1, GWTC-2.1, and GWTC-3 containing candidate gravitational-wave (GW) events detected during its runs O1, O2, and O3. These GW events can be possible sites of neutrino emission. In this paper, we present a search for neutrino counterparts of 90 GW candidates using IceCube DeepCore, the low-energy infill array of the IceCube Neutrino Observatory. The search is conducted using an unbinned maximum likelihood method, within a time window of 1000 s, and uses the spatial and timing information from the GW events. The neutrinos used for the search have energies ranging from a few GeV to several tens of TeV. We do not find any significant emission of neutrinos, and place upper limits on the flux and the isotropic-equivalent energy emitted in low-energy neutrinos. We also conduct a binomial test to search for source populations potentially contributing to neutrino emission. We report a nondetection of a significant neutrino-source population with this test.

Unified Astronomy Thesaurus concepts: Neutrino astronomy (1100); Neutrino telescopes (1105); Gravitational waves (678); Gravitational wave astronomy (675); Particle astrophysics (96)

1. Introduction

Multimessenger astronomy is a growing field, where combined observations with different types of observatories are used to gain more information about various astrophysical sources. In particular, it is an excellent tool to help us nail down the sources of astrophysical neutrinos. The observation of neutrinos with the IceCube Neutrino Observatory (Aartsen et al. 2017) from the direction of a blazar (IceCube Collaboration et al. 2018), TXS 0506+056, followed by electromagnetic (EM) detections of the same source (Aartsen et al. 2018), which thereby boosted its significance, is an excellent example that illustrates the importance of multimessenger observations to identify neutrino sources. While TXS 0506+056 was detected initially in the real-time stream of IceCube, NGC 1068, an obscured active galaxy, was identified as a neutrino source with the help of a catalog of known gamma-ray emitters (Abbasi et al. 2022). The identification of both of these sources demonstrate the power of multimessenger observations.

Binary mergers of black holes (BBH), neutron stars (BNS), and neutron star–black hole (NSBH) are known to produce gravitational waves (GWs). These systems are also considered as possible sites of neutrino production. In particular, relativistic outflows resulting from the merger of BNS and NSBH systems can produce neutrinos in the TeV–PeV energy range. The relativistic protons can also scatter off the slower neutrons within the ejecta and produce GeV neutrinos (Bartos et al. 2013; Murase et al. 2013; Murase & Bartos 2019). The expected neutrino emissivity from a structured jet can vary depending on the jet angle and can be much larger than that from a uniform jet (Ahlers & Halser 2019). It is predicted that the flux of neutrinos (mainly in the few 10–100s of GeV regime) can be enhanced in an off-axis observation scenario, especially when subphotospheric

emission of a gamma-ray burst (GRB) is considered (Biehl et al. 2018). The timescale of neutrino emission from GRBs, which is set as the reference scale for observing neutrinos from binary mergers, is predicted to be $t_{\mathrm{neutrino}} - t_{\mathrm{GW}} \approx \pm 500$ s (Baret et al. 2011). Some models also predict longer timescales for the neutrino emission, in particular from BNS and NSBH mergers (Fang & Metzger 2017).

Several searches in the past have looked for neutrinos correlated with GW detections, with no emission detected so far with high significance. Previous searches from IceCube focused on high-energy neutrinos with energies above several 100s of GeV that can be coincident with the observed GW events (Aartsen et al. 2020; Abbasi et al. 2023a). During the O3 run of LIGO and Virgo, these searches were conducted both in real time—when public alerts of GW events were sent by the LIGO/Virgo Collaboration (LVC)—and offline, once the GW catalogs were published after LVC performed its offline analyses. Archival searches were performed on the GW events from GWTC-1 (Abbott et al. 2019), GWTC-2.1 (Abbott et al. 2021b), and GWTC-3 (Abbott et al. 2021c). No significant emission was found in any of these searches using high-energy neutrinos (Aartsen et al. 2020; Abbasi et al. 2023a). IceCube's search for neutrinos in the MeV–GeV energy range did not return any significant observation and has constrained the neutrino emission from GW sources at these energies (Abbasi et al. 2021). Searches from other detectors like ANTARES (Albert et al. 2020), KamLAND (Abe et al. 2021), Super-Kamiokande (Abe et al. 2021), and Borexino (Agostini et al. 2017) did not yield any significant detection either.

While the emission of neutrinos coincident with GW events has not been detected so far, a counterpart in the EM regime has been confidently observed. GRB170817A, which is the EM counterpart of GW170817, the first BNS event detected by LVC, was observed with gamma-ray telescopes (Abbott et al. 2017) and was later confirmed by optical telescopes to originate from the host galaxy NGC 4993 (Coulter et al. 2017). Spectroscopic observations in the UV, IR, and optical regimes confirmed the EM counterpart to be a kilonova (Coulter et al. 2017; Smartt et al. 2017). Further campaigns established X-ray (Troja et al. 2017) and radio counterparts (Alexander et al. 2017; Hallinan et al. 2017) to GW170817. Neutrinos, however, were not observed in searches conducted by IceCube, ANTARES, and the Pierre Auger Observatory, neither within

[65] also at Institute of Physics, Sachivalaya Marg, Sainik School Post, Bhubaneswar 751005, India.
[66] also at Department of Space, Earth and Environment, Chalmers University of Technology, 412 96 Gothenburg, Sweden.
[67] also at Earthquake Research Institute, University of Tokyo, Bunkyo, Tokyo 113-0032, Japan.

a period of ± 500 s nor within a 14 day period after the merger (Albert et al. 2017). Further searches for coincident observations of GW events and EM/neutrino counterparts have been unsuccessful in obtaining a significant observation, which can mainly be attributed to the relatively large luminosity distances of these GW events (Abbott et al. 2020).

Although previous searches for joint emission from merger events with both IceCube and other neutrino detectors did not return any significant observations, it is worthwhile to search for low-energy neutrinos detected by IceCube that are potentially coming from such a merger. In particular, the different exposure to these class of neutrinos detected with IceCube proves useful.

Here, we present the results of our search for low-energy neutrinos coincident with the candidate GW events published in the LVC catalogs GWTC-1, GWTC-2.1, and GWTC-3 (Abbott et al. 2019, 2021b, 2021c). In Section 2 we describe the IceCube neutrino observatory and its infill array IceCube DeepCore, which detects the low-energy data set used in this analysis. We describe the GW observations used for this follow-up study in Section 3 and the analysis method in Section 4. We show the obtained results in Section 5. Finally, we present the conclusions in Section 6.

2. IceCube and IceCube DeepCore

The IceCube Neutrino Observatory is a cubic-kilometer detector array located at the South Pole (Aartsen et al. 2017), and consists of 86 strings drilled into ice. These strings hold 5160 digital optical modules (DOMS) hosting photomultiplier tubes at depths ranging from 1450 to 2450 m from the surface. The array has a horizontal spacing of 125 m between the strings and a vertical spacing of 17 m between the DOMs. The DOMs are designed to detect signals from Cherenkov photons emitted by charged leptons that are produced by neutrinos interacting with the surrounding medium of ice.

IceCube is also equipped with an infill array, known as DeepCore, which features eight strings with DOMs located at depths of 2100 to 2450 m from the surface (Abbasi et al. 2012). These DOMs have a higher quantum efficiency than those in the main array. This, along with the shorter spacing between the DeepCore strings (72 m) and the individual DOMs on each string (7 m), allows for the detection of lower-energy neutrinos. While the main array of IceCube detects neutrinos with energies above hundreds of GeV, IceCube DeepCore has the capability to detect neutrinos with energies of a few GeV and above.

There are two main types of event signatures observed in IceCube data. Tracks are formed when muon neutrinos undergo charged-current interactions in ice, producing secondary muons that travel in a straight line. Cascades, on the other hand, are event types that involve the charged-current interactions of electron neutrinos resulting in the production of electrons, which in turn produce EM showers in ice. Cascades are also produced by neutral-current interactions of muon, electron, and tau neutrinos in ice. A special class of events appears among cascades and tracks: starting events in which the neutrino interaction occurs inside the detector volume resulting in light detected from an initial hadronic cascade as well as the outgoing lepton.

In this paper, we use a data set with a selection of low-energy neutrinos detected by IceCube DeepCore. This data set, hereby named the (GeV Reconstructed Events with Containment for Oscillation (GRECO) Astronomy data set (Abbasi et al. 2023b), is optimized for low-energy searches of astrophysical transients and contains neutrinos of all flavors with cascade and track event topologies. It consists of starting events observed in IceCube DeepCore, with energies ranging from a few GeV to several tens of TeV. These neutrinos are selected from the entire sky, resulting in similar effective areas for the data set in both the Northern and the Southern Hemispheres. A majority of the events within the data set are either atmospheric neutrinos or atmospheric muons. The data set, however, is suited for searches of transient sources of astrophysical neutrinos since the background is suppressed on short timescales. Unlike the high-energy neutrino data sets, the neutrinos in the GRECO Astronomy data set have worse angular resolution. The angular uncertainties of these events are energy dependent and the median value can be as large as $\sim 50°$ at a few GeV, but can also be as small as $\sim 5°$ at a few hundreds of GeV, especially for starting tracks. The sensitive energy range of the neutrinos in the data set starts at ~ 3 GeV and goes up to ~ 50 TeV. Other data sets have demonstrated better sensitivities for neutrino-source searches than the GRECO Astronomy data set at energies starting from ~ 200 GeV in the Northern Hemisphere and ~ 10 TeV in the Southern Hemisphere. The average rate of the data set is 4.5 mHz. For more details about the GRECO Astronomy data set, see the appendix in Abbasi et al. (2023b).

3. Gravitational-wave Detections from LIGO/Virgo

The Advanced LIGO detectors (LIGO Scientific Collaboration et al. 2015) had their first observing run (O1) from 2015 September 12 to 2016 January 19, followed by their second run (O2) from 2016 November 30 to 2017 August 25. On 2017 August 1 Virgo (Acernese et al. 2015) also joined the observing run, forming a global three-detector system which resulted in better sky localizations than before (Abbott et al. 2019). LVC published the catalog GWTC-1, containing 11 confident detections of GW events from its O1 and O2 observing runs. These events consisted of 10 BBH and one BNS mergers (Abbott et al. 2019). LVC resumed its third observing run (O3) on 2019 April 1. The first half of O3 (known as O3a) ended on 2019 October 1, and the second half (O3b) was conducted from 2019 November 1 to 2020 March 27. The candidate GW events from O3a were published initially in GWTC-2 (Abbott et al. 2021a), which was later updated to the GWTC-2.1 catalog (Abbott et al. 2021b), containing 44 GW events (42 BBH, one BNS, and one NSBH). Following this, LVC also published GWTC-3, a catalog containing the candidate events from O3b (Abbott et al. 2021c). This catalog reported 35 GW events (32 BBH events and three NSBH events) with high astrophysical probability ($p_{astro} > 0.5$) and seven marginal events ($p_{astro} < 0.5$). For these GW events from the catalogs mentioned above, we see that the sky coverage goes down to ~ 20 deg^2 in the case of well-localized GW events, and up to $\sim 20,000$ deg^2 for badly localized events. For more details, see Table 1.

In this paper, we follow up all 11 GW events from GWTC-1, 44 events from GWTC-2.1, and 34 GW events with high p_{astro} along with one marginal GW event (GW200105_162426, previously published as a public alert and an interesting candidate NSBH event) from GWTC-3. GW191222_033537 from GWTC-3 is omitted in this study due to an absence of data within the GRECO Astronomy data set during the period of this merger.

4. Analysis Method

An unbinned maximum likelihood method forms the core of the analysis. For each GW event, we search for neutrinos within a time window of ±500 s. The method is similar to those used in previous high-energy neutrino follow-up searches (Aartsen et al. 2020; Veske et al. 2021).

We define a likelihood of the form

$$\mathcal{L} = \frac{(n_s + n_b)^N}{N!} e^{-(n_s+n_b)} \prod_{i=1}^{N} \left(\frac{n_s \mathcal{S}_i}{n_s + n_b} + \frac{n_b \mathcal{B}_i}{n_s + n_b} \right). \quad (1)$$

Here, n_s is the number of signal events, n_b is the number of background events, N is the observed number of events, $\mathcal{S}_i$ represents the signal probability density function (PDF), and $\mathcal{B}_i$ represents the background PDF. The first term in the likelihood is a Poisson term which accounts for fluctuations in the short time window considered here, and the product term accounts for the probabilities for each event. The Poisson term along with the ±500 s time window results in the likelihood being specialized for transient-source searches. There is no further optimization done on the transient likelihood. That is, a box profile is considered for the time window and we do not consider any particular shape for the time profile of the emission to avoid any model dependence. Moreover, the low event rate of the data set implies that we expect only ≈ 4–5 events on the sky within the 1000 s time window. The signal PDF depends on the energy and the spatial location of the neutrino event, and is derived from Monte Carlo simulations. The energy term is dependent on the spectral index, assuming a simple power-law flux. The background PDF is derived from data by randomizing the events with respect to time. For this, we randomly choose the events within a ±5 day time window with respect to the GW time. This procedure is equivalent to randomizing in R.A., and preserves the seasonal time structure of the data at the same time.

The likelihood defined in Equation (1) is used to formulate the test statistic (TS), which compares a signal and background hypothesis to a background-only hypothesis. The TS is defined as

$$(\text{TS}) = \max. \left\{ 2 \ln \left(\frac{\mathcal{L}_k(n_s, \gamma) \cdot w_k}{\mathcal{L}_k(n_s = 0)} \right) \right\}, \quad (2)$$

where γ is the spectral index, which is allowed to float in the fit. The entire sky is divided into 49,152 pixels as a HEALpix grid (Górski et al. 2005; with nside = 64) for this procedure. Here w_k is a spatial weighting term applied to each pixel k in the sky, and is calculated as the ratio of the GW probability in each pixel and the area of the pixel, normalized across the whole sky. The term $2 \ln(w_k)$ has a maximum value of 0 corresponding to the maximum probability pixel in the sky and has negative values at other pixels. The probabilities are obtained from the HEALpix skymap of the GW event. The likelihood ratio is evaluated at each pixel covering 99.99% of the GW probability map and the TS value is taken as the maximum from such a scan over the pixels (Balagopal et al. 2021).

The procedure is used to evaluate the TS distribution of the background-only hypothesis, and also the distributions for pseudoexperiments with signal injections. The background TS distribution is also used to compute the observed one-sided p-

(a)

(b)
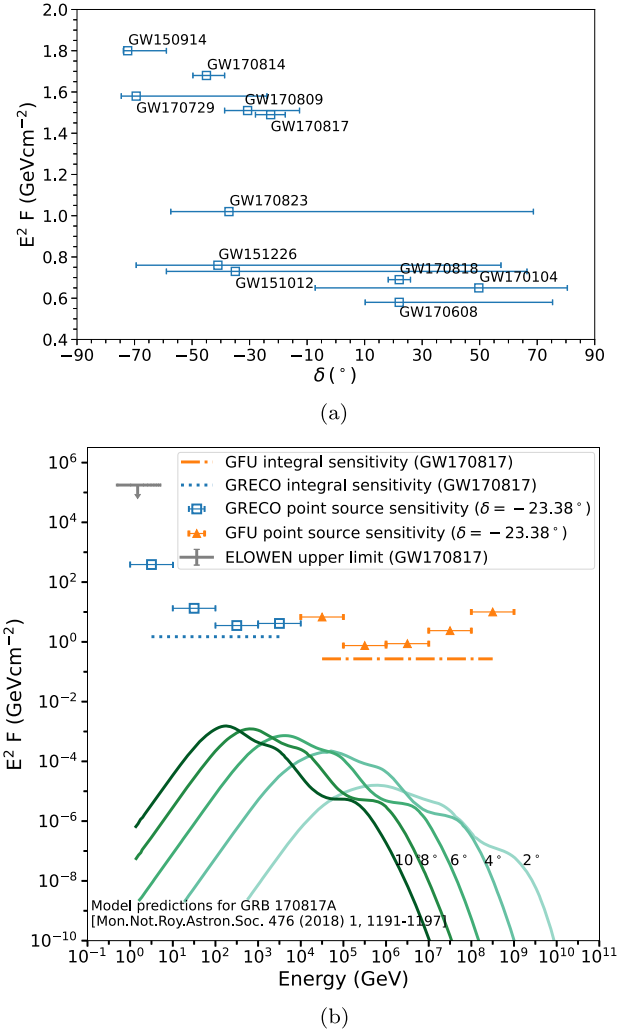
Figure 1. (a) Sensitivities of the GRECO Astronomy data set to the 11 GW events in the GWTC-1 catalog. The x-axis represents the decl. of the corresponding GW events (decl. with maximum probability shown by the squares and the decl. covering the 68% probability region shown as error bars). F represents the time-integrated flux as defined in Equation (3). The sensitivities for events in the Northern and Southern Hemispheres are within an order of magnitude. (b) The differential sensitivities of the GRECO Astronomy data set (in blue squares) compared to the differential sensitivities of the high-energy data set (GFU). The differential sensitivity curves are constructed by dividing the entire energy range into decadal bins. The GRECO Astronomy data set contains neutrinos of all flavors while GFU contains only muon neutrinos. Also shown are the integral sensitivities to a decl. corresponding to that of the host galaxy of GW170817, NGC 4993 (Coulter et al. 2017). The gray marker shows the flux upper limit on GW170817 obtained with the follow-up analysis using extremely low-energy neutrinos detected with IceCube (Abbasi et al. 2021). The green curves represent model predictions showing low-energy neutrino emission from a GRB like 170817A (Biehl et al. 2018). All sensitivities shown in (a) and (b) assume a spectral index of two for the flux.

values reported in Section 5. The sensitivity is calculated from these TS distributions. We define the sensitivity as the flux level at which 90% or more of the signal-injected pseudoexperiments return a TS value greater than the median TS of the background distribution. For more details of the sensitivity calculations see Balagopal et al. (2021).

Figure 1 shows the sensitivities obtained with this analysis. The sensitivity for each GW event in the GWTC-1 catalog is shown in Figure 1(a). These are the sensitivities where spatial constraints are also included for each GW event. The

corresponding decl. covered by the GW events are shown on the x-axis. We define the time-integrated flux (per flavor), shown in Figures 1(a) and (b), as

$$F = \frac{dN}{dE\,dt\,dA}\Delta t = \phi_0 \cdot \left(\frac{E}{E_0}\right)^{-\gamma}\ [\mathrm{GeV}^{-1}\,\mathrm{cm}^{-2}], \qquad (3)$$

where N is the number of events, E is the energy, t is the time, A is the area, and $\Delta t = 1000\,\mathrm{s}$ is the time window considered for the neutrino search. ϕ_0 is the flux normalization at the reference energy $E_0 = 1\,\mathrm{GeV}$. We fix the spectral index γ to two for the reported sensitivities and upper limits in this paper, although we allow γ to float within the fit during the likelihood maximization. A detailed study where we fix γ to several choices of values in the likelihood demonstrated that the chosen γ does not affect the reported flux values, since this is a short time window search and therefore behaves close to a counting experiment where the choice of spectral index does not affect the analysis. The Northern and the Southern sky behavior of the sensitivities of the GRECO Astronomy data set is evident from Figure 1(a). While the Southern sky sensitivity is worse than that of the Northern sky (which is expected, due to the higher atmospheric background in the Southern sky), they remain within the same order of magnitude. It is seen that for events with large coverage across the sky, shown as large error bars on the decl. in Figure 1(a), an averaging of the point-source sensitivities at the decl. range it spans occurs. For smaller skymaps the sensitivity becomes identical to the point-source sensitivity at that decl.

A comparison of the sensitivities of the different data sets within IceCube, which cover different energy ranges, used to search for neutrinos correlated to GW events, is shown in Figure 1(b). The differential sensitivities shown in the figure are calculated within each decadal energy bin using the same method as that for the integral sensitivities, by restricting the the energy to the corresponding ranges. A spectral index of two is assumed within each energy bin. While the sensitivity for high-energy neutrinos (GFU data set; IceCube Collaboration et al. 2016; Kintscher & IceCube Collaboration 2016) is better within IceCube, it is evident from the figure that the GRECO Astronomy data set provides complementary information at lower energies, which is otherwise inaccessible. Also notice-able are the similar sensitivities (differential) of the lowest energy bin of the GFU data set and the highest energy bin of the GRECO Astronomy data set. The differential sensitivity for the GRECO Astronomy data set shown in the figure corresponds to $\delta = -23.38°$. The differential sensitivities for positive decl. and at the horizon follow similar trends to what is shown in the figure. This is unlike the differential sensitivities for the GFU data set, which vary a lot between the Northern and Southern Hemispheres. For a comparison of the differential sensitivities of the two data set at various decl. see the appendix of Abbasi et al. (2023b). The upper limit obtained with ELOWEN, an extremely low energy search with IceCube (Abbasi et al. 2021), is also shown in the figure and is seen to be orders of magnitude above the sensitivity of the GRECO Astronomy data set.

Model predictions for the possible emission of low-energy neutrinos from BNS mergers from Biehl et al. (2018) are also shown in Figure 1(b). This model was formulated based on GRB170817A, which is the observed gamma-ray counterpart to GW170817. The curves depict off-axis emission for a fixed assumption of the Lorentz factor ($\Gamma = 30$) and baryonic loading ($\xi = 100$). The various curves represent different observation angles ($2°$, $4°$, $6°$, $8°$, and $10°$ from right to left), where the observation angle is the angle between the edge of the jet and the observation axis. Here, only the curves for the subphotospheric emission from the original paper are shown (Biehl et al. 2018). For comparison, the observation angle for GRB170817A is estimated to be $\sim 28°$ (Troja et al. 2017). Although the model relates to the specific case of GW170817, this is relevant for other GWs also, since off-axis observations are more likely than on-axis observations. The flux of neutrinos from such sources can also scale up or down depending on the Lorentz factor, as shown in Biehl et al. (2018). These model predictions are shown only to depict the relative scales of IceCube sensitivities and expected emission from such sources. There are several other possible emission scenarios discussed in other papers (Ahlers & Halser 2019; Carpio & Murase 2020; Gottlieb & Globus 2021). From the figure, it is evident that such model predictions are ~ 3 orders of magnitude below the sensitivities of IceCube. Even in the large observation angle scenario, the GRECO Astronomy sensitivities (assuming a source-spectral shape of E^{-2}) are well above the model predictions. Conducting searches as described in this analysis could help test such models. A significant detection of neutrinos could hint toward an incomplete understanding of the physics of neutrino production in such sources.

4.1. Population Test

In addition to conducting individual follow ups for each GW event, we also perform a binomial test to search for a source population. This test is conducted only on the GW events with high astrophysical probability reported by LVC (89 out of 90 events). To conduct the binomial test, we first order the observed p-values for the 89 GW events in their ascending order. After choosing the first k GW events out of these, we then calculate the binomial probability to obtain m successes given by

$$P(k) = \sum_{m=k}^{N} \frac{N!}{(N-m)!m!}p_k^m(1-p_k)^{(N-m)}. \qquad (4)$$

Once we repeat this for $k = 1$ to $k = 89$, we choose the lowest value of $P(k)$ and this is the final binomial probability (pretrial).

To account for the trials factor for this test, we perform the binomial test on the background-only scenario. We randomly pick TS values from the background-only TS distribution of the 89 GW events and calculate the corresponding binomial p-value. This is repeated multiple times to construct a background distribution of binomial p-values. The observed binomial p-value can be compared to this background distribution to correct for the trials.

5. Results

The search for neutrinos within a 1000 s time window is conducted for 90 GW events from GWTC-1, GWTC-2.1, and GWTC-3. No significant emission is seen for any GW event. The GW event with the lowest pretrial p-value is found to be GW151226, which is a BBH event. The GW events are treated as three separate groups of BBH, BNS, and NSBH for trials-correction purposes. The pretrial p-value of GW151226 is 7.83×10^{-3} (2.4σ), which becomes 4.83×10^{-1} after correcting for trials run for 83 BBH events. Out of the BNS candidate

Table 1
The Obtained Results for the 90 GW Events Followed Up in This Analysis

GW	Type	Area (deg^2)	Distance (Mpc)	p-value	Upper Limit ($E^2 F$) (GeV cm^{-2})	E_{iso} U. L. (erg)
GW151226	BBH	1039.0	450	7.83×10^{-3}	3.80	3.10×10^{54}
GW190910_112807	BBH	10,880.3	1460	3.07×10^{-2}	3.04	3.74×10^{55}
GW200316_215756	BBH	410.4	1120	3.79×10^{-2}	1.71	4.47×10^{54}
GW190630_185205	BBH	1216.9	890	4.12×10^{-2}	2.83	1.21×10^{55}
GW190426_190642	BBH	8214.5	4350	4.13×10^{-2}	2.80	3.03×10^{56}
GW190413_052954	BBH	1484.5	3550	4.23×10^{-2}	2.05	1.62×10^{56}
GW170823	BBH	1650.0	1940	5.07×10^{-2}	2.59	3.57×10^{55}
GW191230_180458	BBH	1012.2	4300	5.47×10^{-2}	2.94	6.79×10^{55}
GW190930_133541	BBH	1679.6	760	5.48×10^{-2}	1.36	6.05×10^{54}
GW190728_064510	BBH	395.5	870	6.72×10^{-2}	1.98	6.83×10^{54}
GW191216_213338	BBH	480.1	340	6.93×10^{-2}	2.62	2.85×10^{53}
GW190425	BNS	9958.2	160	9.08×10^{-2}	2.49	2.82×10^{53}
GW200129_065458	BBH	81.8	900	9.25×10^{-2}	1.56	2.36×10^{54}
GW200220_061928	BBH	3484.7	6000	1.03×10^{-1}	2.26	1.16×10^{56}
GW190731_140936	BBH	3387.3	3300	1.05×10^{-1}	2.73	1.40×10^{56}
GW170818	BBH	40.3	1060	1.23×10^{-1}	0.88	7.56×10^{54}
GW190503_185404	BBH	94.4	1450	1.24×10^{-1}	2.44	2.26×10^{55}
GW190421_213856	BBH	1211.5	2880	1.26×10^{-1}	2.40	8.32×10^{55}
GW200308_173609	BBH	18,705.7	5400	1.49×10^{-1}	2.38	1.61×10^{56}
GW191103_012549	BBH	2519.6	990	1.58×10^{-1}	1.24	2.29×10^{54}
GW170814	BBH	88.1	600	1.83×10^{-1}	2.07	2.41×10^{54}
GW190925_232845	BBH	1233.5	930	1.84×10^{-1}	1.67	6.64×10^{54}
GW190412	BBH	20.9	740	1.91×10^{-1}	0.70	2.89×10^{54}
GW190521_074359	BBH	546.5	1240	2.17×10^{-1}	0.96	8.95×10^{54}
GW190805_211137	BBH	3949.1	5310	2.53×10^{-1}	1.59	2.78×10^{56}
GW190517_055101	BBH	473.3	1860	2.72×10^{-1}	1.70	2.63×10^{55}
GW200220_124850	BBH	3168.9	4000	2.77×10^{-1}	1.46	4.13×10^{55}
GW190514_065416	BBH	3009.7	4130	2.78×10^{-1}	0.94	1.04×10^{56}
GW190915_235702	BBH	396.9	1620	3.05×10^{-1}	0.59	1.30×10^{55}
GW190916_200658	BBH	4499.2	4460	3.15×10^{-1}	1.33	1.87×10^{56}
GW200112_155838	BBH	4250.4	1250	3.50×10^{-1}	1.56	3.13×10^{54}
GW190828_063405	BBH	520.1	2130	3.59×10^{-1}	1.28	2.58×10^{55}
GW190803_022701	BBH	1519.5	3270	3.71×10^{-1}	0.79	6.62×10^{55}
GW190917_114630	NSBH	2050.6	720	3.84×10^{-1}	1.12	4.06×10^{54}
GW190707_093326	BBH	1346.0	770	3.88×10^{-1}	1.21	3.45×10^{54}
GW190403_051519	BBH	5589.4	8000	4.13×10^{-1}	0.98	2.40×10^{56}
GW191126_115259	BBH	1514.5	1620	4.61×10^{-1}	0.94	3.36×10^{54}
GW200322_091133	BBH	31,571.1	3600	5.15×10^{-1}	0.95	7.44×10^{55}
GW191113_071753	BBH	2993.3	1370	8.15×10^{-1}	1.38	4.67×10^{54}
GW191215_223052	BBH	595.8	1930	8.48×10^{-1}	1.37	6.73×10^{54}
GW190602_175927	BBH	694.5	2690	8.52×10^{-1}	1.65	5.28×10^{55}
GW200105_162426	NSBH	7881.8	270	8.55×10^{-1}	0.77	9.05×10^{52}
GW200225_060421	BBH	509.0	1150	8.55×10^{-1}	0.68	2.21×10^{54}
GW190521	BBH	1008.2	3920	8.65×10^{-1}	1.48	7.27×10^{54}
GW200306_093714	BBH	4371.2	2100	8.66×10^{-1}	0.68	7.08×10^{54}
GW191127_050227	BBH	1499.2	3200	8.69×10^{-1}	0.86	2.31×10^{55}
GW190620_030421	BBH	7202.1	2810	8.71×10^{-1}	0.91	6.16×10^{55}
GW200209_085452	BBH	924.5	3400	8.73×10^{-1}	0.78	2.03×10^{55}
GW200210_092254	BBH	1830.7	940	8.74×10^{-1}	1.21	1.65×10^{54}
GW190706_222641	BBH	653.8	4420	8.78×10^{-1}	0.72	1.27×10^{56}
GW190519_153544	BBH	857.1	2530	8.78×10^{-1}	0.88	3.39×10^{55}
GW150914	BBH	184.6	440	8.79×10^{-1}	1.80	1.13×10^{54}
GW190814	BBH	19.3	240	8.87×10^{-1}	1.4	2.49×10^{53}
GW190719_215514	BBH	2890.1	3940	8.88×10^{-1}	0.81	6.98×10^{55}
GW190408_181802	BBH	148.8	1550	8.91×10^{-1}	0.59	1.10×10^{55}
GW200115_042309	NSBH	511.9	290	8.92×10^{-1}	1.28	1.23×10^{53}
GW200219_094415	BBH	702.1	3400	8.97×10^{-1}	1.38	2.41×10^{55}
GW190727_060333	BBH	833.8	3300	8.98×10^{-1}	1.33	5.96×10^{55}
GW190720_000836	BBH	463.4	790	9.02×10^{-1}	1.15	6.58×10^{54}
GW190708_232457	BBH	13,675.4	880	9.04×10^{-1}	0.72	3.95×10^{54}
GW170817	BNS	31.9	40	9.07×10^{-1}	1.48	7.07×10^{51}
GW170729	BBH	1032.3	2840	9.08×10^{-1}	1.58	5.15×10^{55}
GW200208_130117	BBH	38.0	2230	9.10×10^{-1}	1.55	8.78×10^{54}
GW190513_205428	BBH	518.4	2060	9.10×10^{-1}	0.54	1.56×10^{55}
GW190701_203306	BBH	46.1	2060	9.11×10^{-1}	1.20	2.05×10^{55}
GW190725_174728	BBH	2292.5	1050	9.13×10^{-1}	1.07	6.65×10^{54}
GW190828_065509	BBH	664.0	1600	9.15×10^{-1}	1.50	1.50×10^{55}
GW200128_022011	BBH	2677.5	3400	9.17×10^{-1}	1.06	1.58×10^{55}
GW151012	BBH	1554.3	1080	9.17×10^{-1}	0.65	4.30×10^{54}
GW200224_222234	BBH	49.9	1710	9.19×10^{-1}	1.29	4.92×10^{54}
GW170809	BBH	340.7	1030	9.26×10^{-1}	1.51	4.78×10^{54}
GW191204_171526	BBH	344.9	650	9.28×10^{-1}	1.24	5.62×10^{53}

Table 1
(Continued)

GW	Type	Area (deg^2)	Distance (Mpc)	p-value	Upper Limit ($E^2 F$) (GeV cm^{-2})	E_{iso} U. L. (erg)
GW190924_021846	BBH	357.9	570	9.29×10^{-1}	0.80	1.43×10^{54}
GW170104	BBH	935.8	990	9.34×10^{-1}	0.65	4.31×10^{54}
GW190527_092055	BBH	3662.4	2490	9.34×10^{-1}	1.08	3.33×10^{55}
GW191129_134029	BBH	848.3	790	9.36×10^{-1}	1.16	9.4×10^{53}
GW191105_143521	BBH	728.7	1150	9.38×10^{-1}	1.16	1.89×10^{54}
GW200202_154313	BBH	159.3	410	9.38×10^{-1}	0.25	2.63×10^{53}
GW200208_222617	BBH	1889.2	4100	9.43×10^{-1}	0.78	3.93×10^{55}
GW200311_115853	BBH	35.6	1170	9.44×10^{-1}	1.25	2.17×10^{54}
GW190926_050336	BBH	2505.9	3780	9.44×10^{-1}	1.12	1.27×10^{56}
GW191219_163120	NSBH	2232.1	550	9.53×10^{-1}	0.96	4.60×10^{53}
GW190413_134308	BBH	730.6	4450	9.54×10^{-1}	1.21	1.23×10^{56}
GW190512_180714	BBH	218.0	1430	9.56×10^{-1}	1.27	1.40×10^{55}
GW200302_015811	BBH	7010.8	1480	9.58×10^{-1}	1.04	3.69×10^{54}
GW191109_010717	BBH	1784.3	1290	9.63×10^{-1}	1.28	2.66×10^{54}
GW190929_012149	BBH	2219.3	2130	9.66×10^{-1}	0.83	8.66×10^{55}
GW191204_110529	BBH	4747.7	1800	9.85×10^{-1}	0.84	6.52×10^{54}
GW200216_220804	BBH	3009.5	3800	9.86×10^{-1}	0.52	2.46×10^{55}
GW170608	BBH	538.8	320	1.0	0.58	5.08×10^{53}

Note. The obtained p-values and flux upper limits assuming a spectral index $\gamma = 2$ are shown. The events are ordered with respect to their obtained p-values. The table also shows the upper limits (U. L.) on the total isotropic-equivalent energy emitted in neutrinos with energies between 3 GeV and 50 TeV in this analysis. The distances reported in this table are the mean distances to the GW source marginalized across the whole sky, and is also used in Figure 5. The areas of the GW events are obtained from the sky localizations of the 90% probability regions of the GW skymaps.
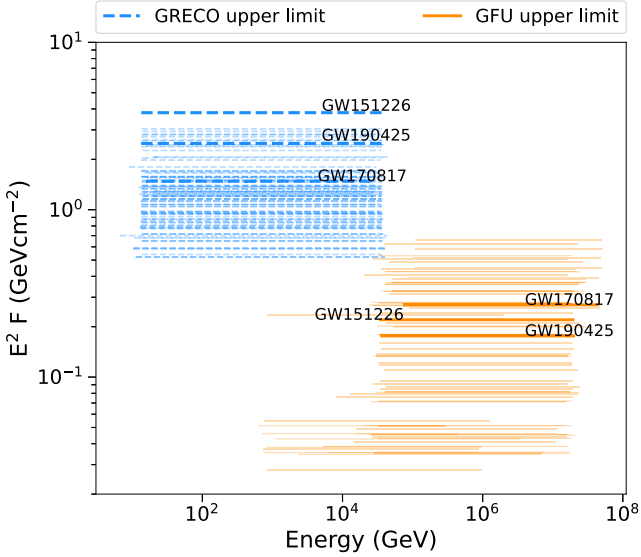
Figure 2. Flux upper limits obtained for the 90 GW events obtained in this analysis (blue dashed). The corresponding flux upper limits obtained with the high-energy neutrino follow-up analysis are also shown (orange solid; Aartsen et al. 2020; Abbasi et al. 2023a). These limits are for a flux with a spectral index of two. The energy ranges shown here are the central 90% energies contributing to the flux limits at the decl. spanning the 90% probability regions of the GW skymap. These energy ranges are computed for each decl. bin by calculating the upper and lower energy limits of the data set at which the sensitivity degrades by 90%. Three GW events are highlighted here. These are GW151226 (the event with the lowest pretrial p-value in this analysis), GW190425 (the only BNS event with a pretrial p-value < 0.1), and GW170817 (first and only BNS event for which the EM counterpart has been observed).

events, GW190425 has the smallest pretrial p-value of 9.08×10^{-2}. Table 1 shows the p-values and the flux upper limits obtained for all 90 GW events followed up in this analysis.

Figure 2 shows the 90% C.L. flux upper limits obtained with the GRECO Astronomy data set for the 90 GW events, assuming a spectral index of two. These upper limits are

compared to those obtained with the high-energy neutrino data set of IceCube. From the figure, it is evident that while the GRECO Astronomy data set can probe energies lower than the GFU data set, its resulting flux upper limits are less constraining, which is primarily due to its worse sensitivities. There are certain GW events with some overlap in the energy ranges probed by the two data sets. These are the GW events that lie mainly in the Northern sky, where the central energy range is lower for the GFU data set when compared to that at the Southern sky. On the other hand, the extent of energies covered by the GRECO data set does not vary a lot between the Northern and the Southern Hemispheres. The flux upper limits with the GFU data set were reported in Aartsen et al. (2020) and Abbasi et al. (2023a).

The figure also highlights three GW events: GW151226 is the event with the lowest pretrial p-value obtained with the GRECO Astronomy data set. Therefore, its flux upper limit is the highest among the 90 tested GW events. GW190425 is the BNS event with the lowest pretrial p-value, and GW170817 is the only BNS event, observed during the O1 run, which also had an EM counterpart. There are no observed neutrino counterparts to GW170817 in both the high-energy and low-energy follow ups.

The distribution of pretrial p-values obtained with the GRECO Astronomy data set is shown in Figure 3. These are the observed p-values for 90 GW events from GWTC-1, GWTC-2.1, and GWTC-3. The background expectations of the p-values for these GW events are also shown in the figure. The background expectation is derived by randomly choosing entries from the background TS distribution of each GW event. The observed p-value distribution is consistent with the background expectation. It is bimodal in nature, a characteristic resulting from the discrete behavior of the TS distribution. This discreteness arises due to the counting experiment done here in a low-background regime.
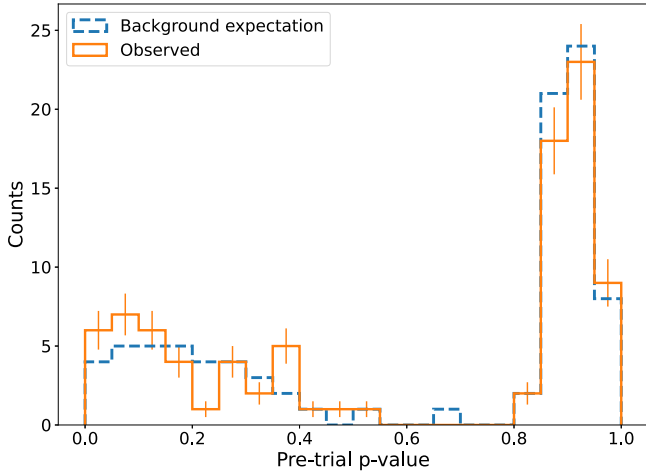
Figure 3. Pretrial *p*-value distribution of the 90 GW events followed up in this analysis (orange solid). This is compared to the background expectation of *p*-values (blue dashed). The observed *p*-value distribution is consistent with the background expectation.
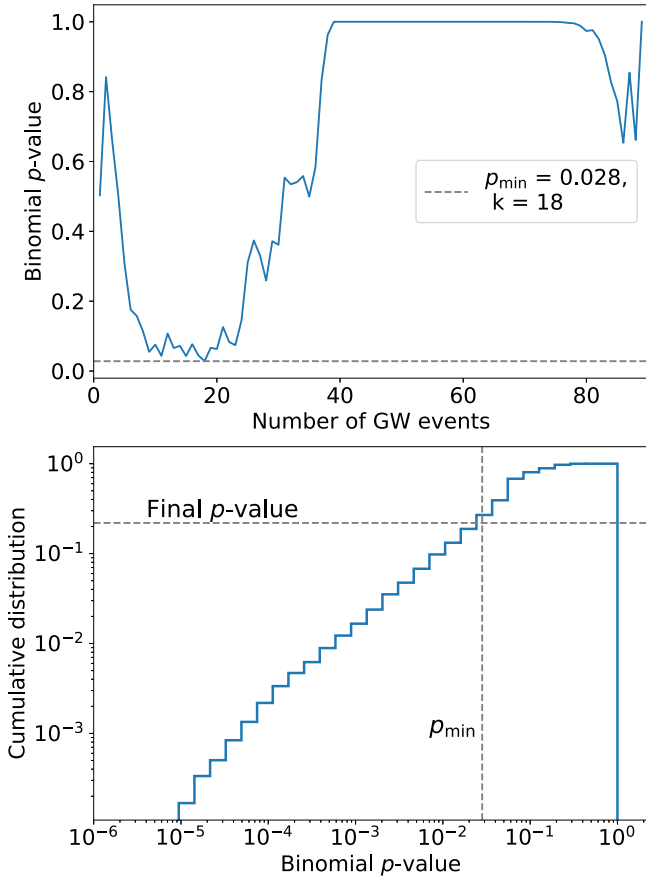
Figure 4. A binomial test is conducted on 89 GW events with high astrophysical probabilities. The top panel shows the evolution of the binomial *p*-value as we add *k* GW events (*x*-axis), sorted according to their pretrial *p*-values. The minimum value, $p_{min} = 0.028$, is the resultant binomial *p*-value of this population test and is obtained from 18 GW events. The bottom panel shows the trials-correction procedure for the binomial test. p_{min} (dashed vertical line) is compared to the background distribution of binomial *p*-values (blue histogram) and corrected for, based on its probability of occurrence. This results in the final, trial-corrected, *p*-value of 0.215 (dashed horizontal line).

We perform a binomial test on the collection of GW events with high astrophysical probability followed up in this analysis in order to test the existence of a population of a combined GW
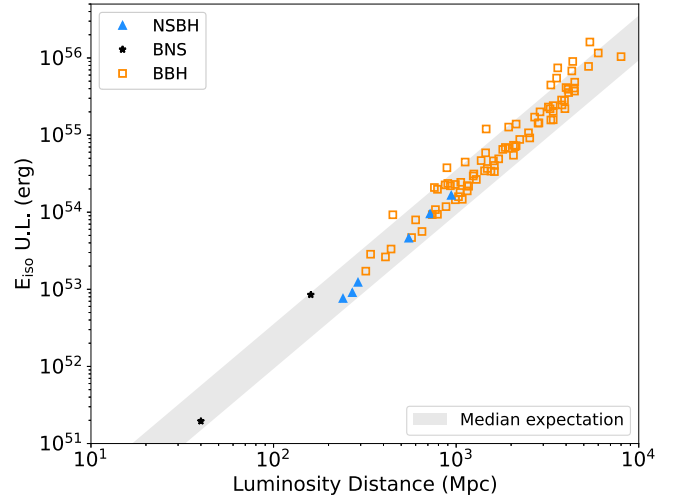
Figure 5. Upper limits to the isotropic-equivalent energy emitted in low-energy neutrinos of all flavors. The orange squares show the BBH events, the blue triangles show the NSBH events, and the black stars show the BNS events. Also shown is the median expectation of the E_{iso} upper limits, derived from the background sensitivities of the GRECO Astronomy data set (gray band). The events that lie above the band are those with *p*-values <0.1 seen in this analysis. Also note that the observed isotropic energy in gamma rays from GRB170817A is 1.36×10^{46} erg, which is several orders of magnitude below the scale of this figure. The corresponding event GW170817 is the bottom-left star in this figure.

and neutrino source, as described in detail in Section 3. We obtain a binomial *p*-value of 2.8×10^{-2} corresponding to a population of 18 GW events. The observed binomial *p*-value is compared to the background distribution of binomial *p*-values to obtain a posttrial *p*-value of 2.15×10^{-1}. Figure 4 shows the results of the binomial test.

The observed TS values for each GW event are used to place an upper limit on the isotropic-equivalent energy (E_{iso}) emitted in neutrinos of all flavors. For each GW event, we determine the required E_{iso} to produce the observed TS value in 90% of the injected pseudoexperiments. E_{iso} is related to the flux of neutrinos by the equation

$$\frac{E_{iso}}{4\pi r^2} = \int_{E_1}^{E_2} \Phi(E) E \, \Delta t \, dE, \tag{5}$$

where $\Phi(E)$ is the flux of neutrinos and r is the distance from the source. We compute E_1 as 3 GeV and E_2 as 50 TeV for the GRECO Astronomy data set, which is the sensitive energy range of the data set for a source spectrum of the shape E^{-2} and is calculated in the same manner as the energy ranges depicted in Figure 2. With this, a given E_{iso} is converted to neutrinos detected at IceCube after convolving with the 3D location of the source, which is marginalized, and the decl.-dependent effective areas of the data set. For more details of the method see Aartsen et al. (2020). The source-location information was obtained from the data release from LVC (LIGO Scientific Collaboration & Virgo Collaboration 2019, 2021; LIGO Scientific Collaboration et al. 2021).

The E_{iso} upper limits obtained with this analysis are shown in Figure 5. The figure shows 90 GW events from GWTC-1, GWTC-2.1, and GWTC-3. The trend of increasing upper limits on E_{iso} as the luminosity distance increases is to be expected based on a $4\pi r^2$ spherically-symmetric emission. Most of the events lie within the bounds for the median E_{iso} expectation,

shown as a band in the figure. It is seen that some observed $E_{\rm iso}$ upper limits lie above the gray band. These events correspond to the events with pretrial p-values < 0.1 and therefore have a high TS, which is expected to occur when many experiments are conducted. A higher observed TS, in turn, leads to less stringent upper bounds on $E_{\rm iso}$. These events are consistent with the 3σ expectations from the background and therefore they do not indicate a significant population. The reported $E_{\rm iso}$ upper limits assume a source spectrum of the form E^{-2}.

6. Conclusion

We have presented the results of a search for low-energy neutrinos detected with IceCube DeepCore that are coincident with GW events detected by LVC. The data set used here includes neutrinos of all flavors. The search was conducted for 90 GW events in a 1000 s time window centered around the time of each GW event, and did not result in any significant detection. We have also performed a binomial test to search for the existence of an underlying population of neutrinos associated with GW events. We report a posttrial p-value of 2.15×10^{-1} for this test. Further, we set flux upper limits and $E_{\rm iso}$ upper limits for each GW event used in this study.

The results presented here complement those from the high-energy neutrino follow up (Aartsen et al. 2020; Abbasi et al. 2023a) and the extremely low-energy neutrino search (Abbasi et al. 2021) previously published by IceCube. We note that some of the GW events have an observed pretrial p-value $\leqslant 0.1$ in the analysis presented here as well as the previously published IceCube search with high-energy neutrinos. However, it is not appropriate simply to multiply the p-values obtained from the two searches. There are some neutrino events that are common in both data sets. Also, due to the large spatial localizations of the GW events it is natural that accidental coincidence of the GW skymap with the neutrino events from both data sets occur, sometimes at disjointed locations in the sky. An analysis that addresses all of these factors and does a combined search including both data sets will be performed to understand the possible emission across a wide energy range from these GW events in a robust manner.

With the expected increase in the GW detection rate from the next run of the LIGO/Virgo/KAGRA (LVK) collaboration, more GW events will be available for searches like that presented in this paper, allowing us to probe more possibilities of joint emission. A better localization of the GW sources will also enhance such a search. The GRECO Astronomy data set is expected to exhibit improved reconstruction with the use of more advanced methods like those including neural networks. This can further improve the significance of a possible joint emission.

In addition to this, IceCube Upgrade—the upcoming enhancement to the infill array—will provide a higher exposure at low energies and is expected to improve the localization and energy determination capabilities of the detector at lower energies. This is also expected to improve the capabilities of the analysis presented in this paper.

Appendix
Skymaps

The skymaps of the 90 GW events followed up in this paper and the corresponding neutrinos within the GRECO Astronomy data set within the 1000 s time windows are shown here in Figures 6–8.
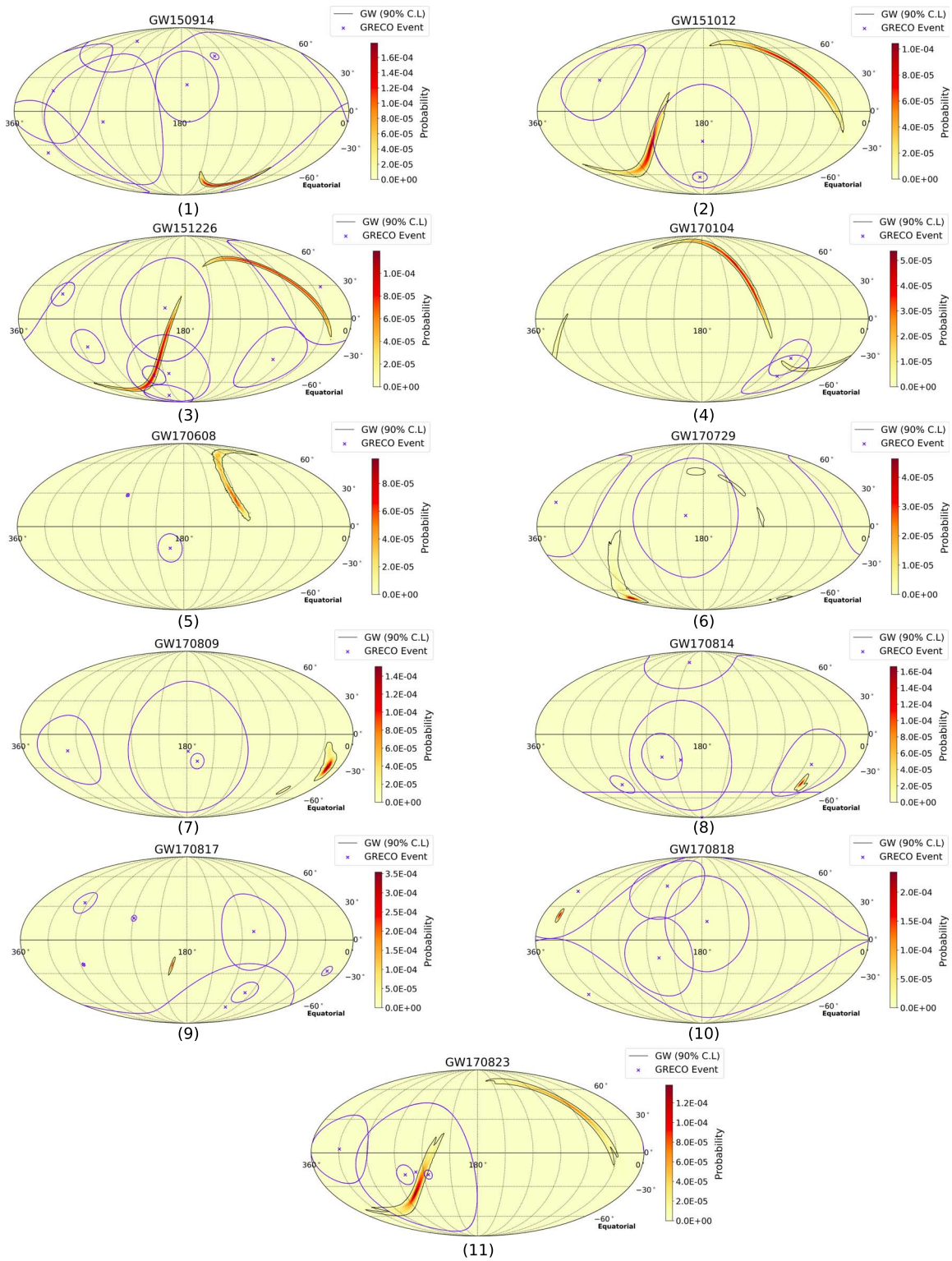
Figure 6. The skymaps for the GW events in GWTC-1 and the neutrino events observed within the 1000 s time window (1–11).
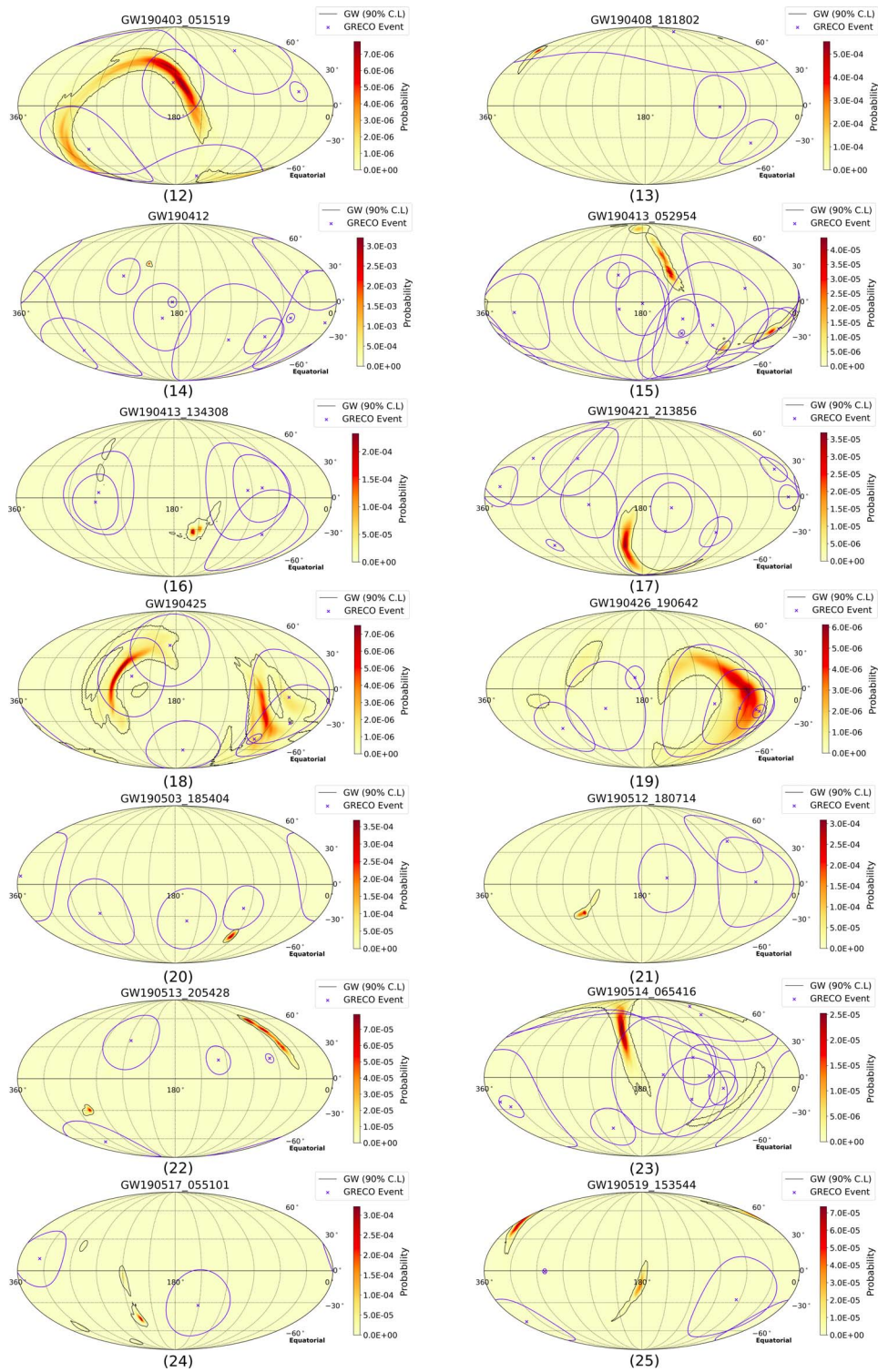
Figure 7. The skymaps for the GW events in GWTC-2.1 and the neutrino events observed within the 1000 s time window (12–55).
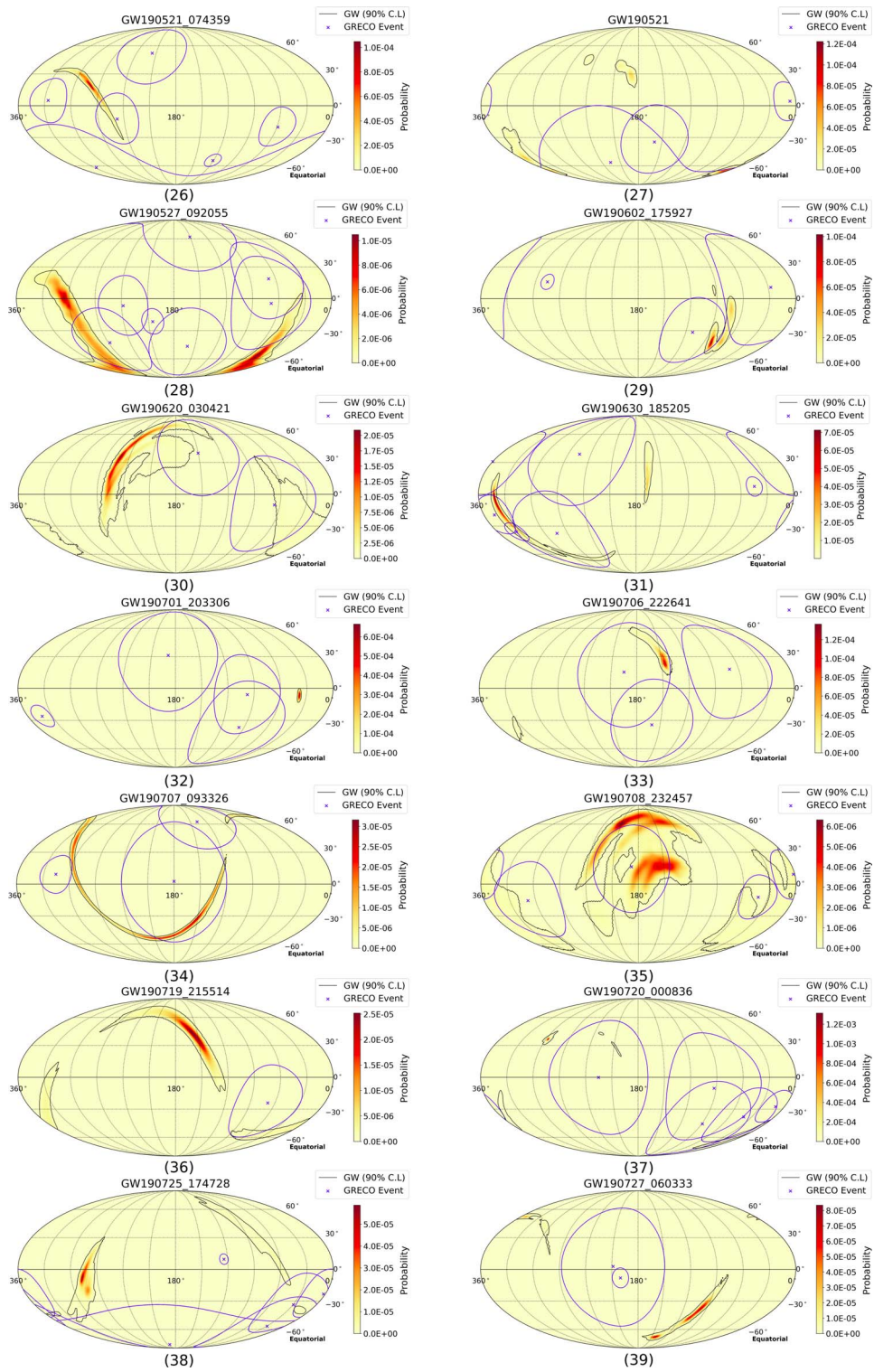
Figure 7. (Continued.)
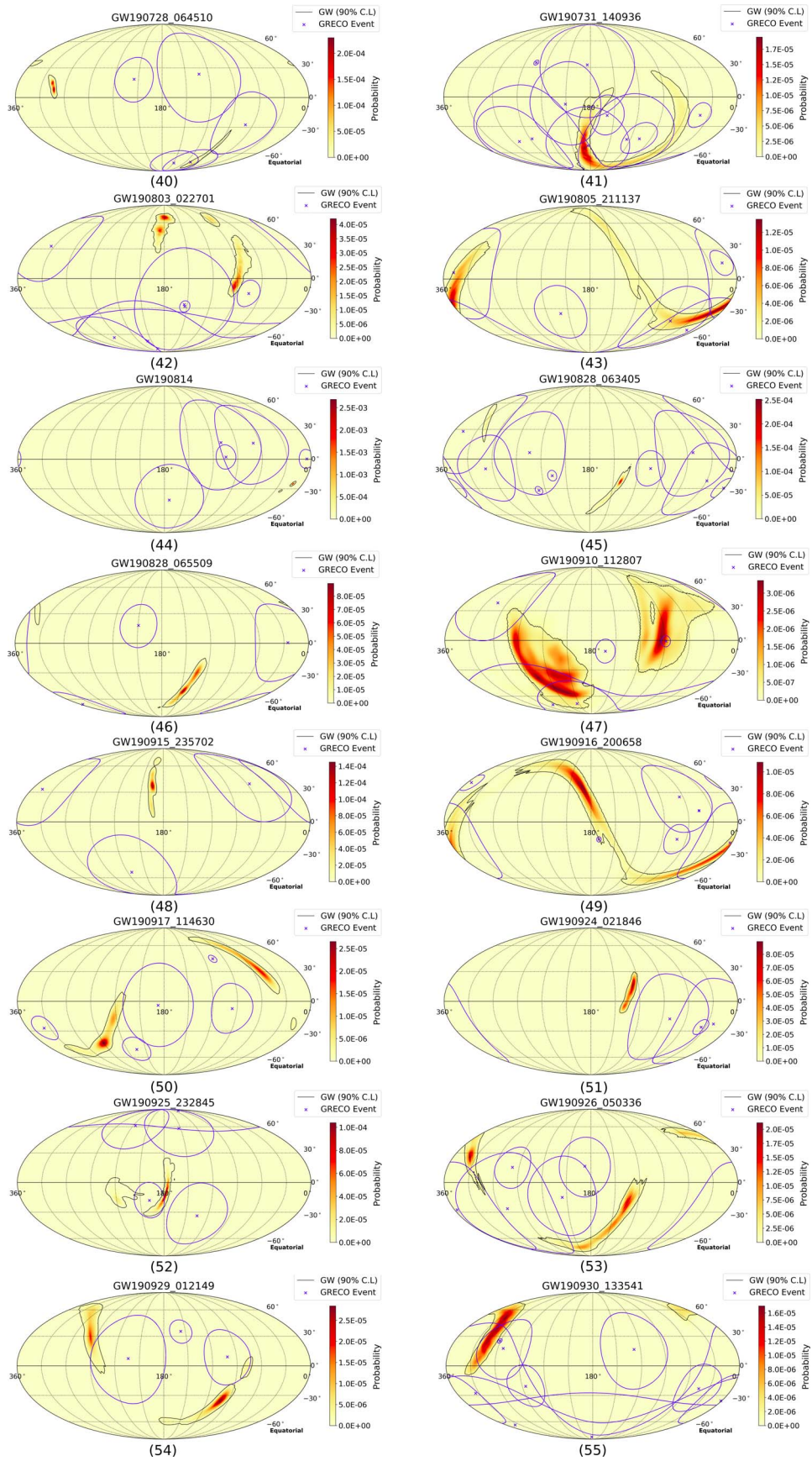
Figure 7. (Continued.)
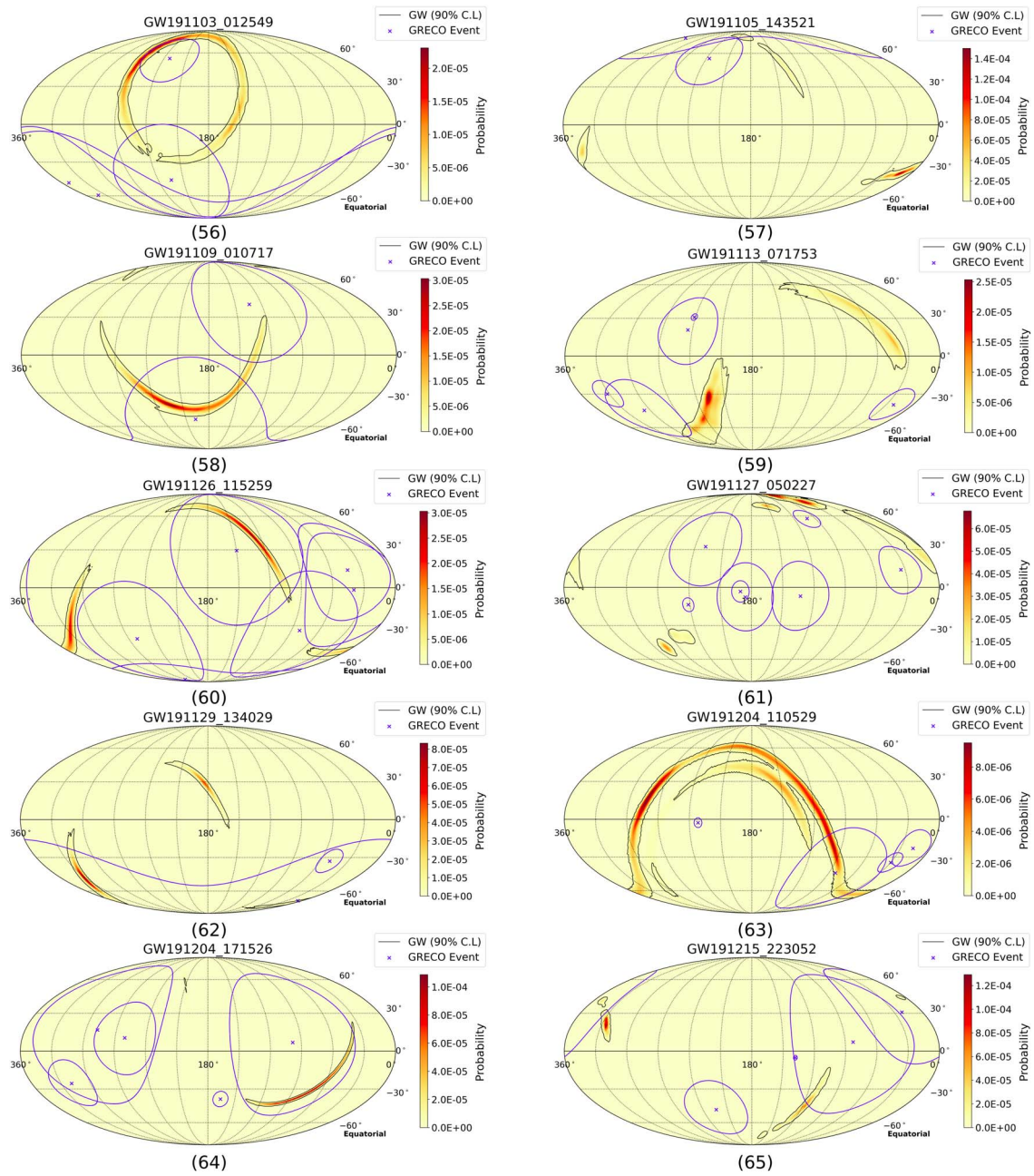
Figure 8. The skymaps for the GW events in GWTC-3 and the neutrino events observed within the 1000 s time window (56–90).
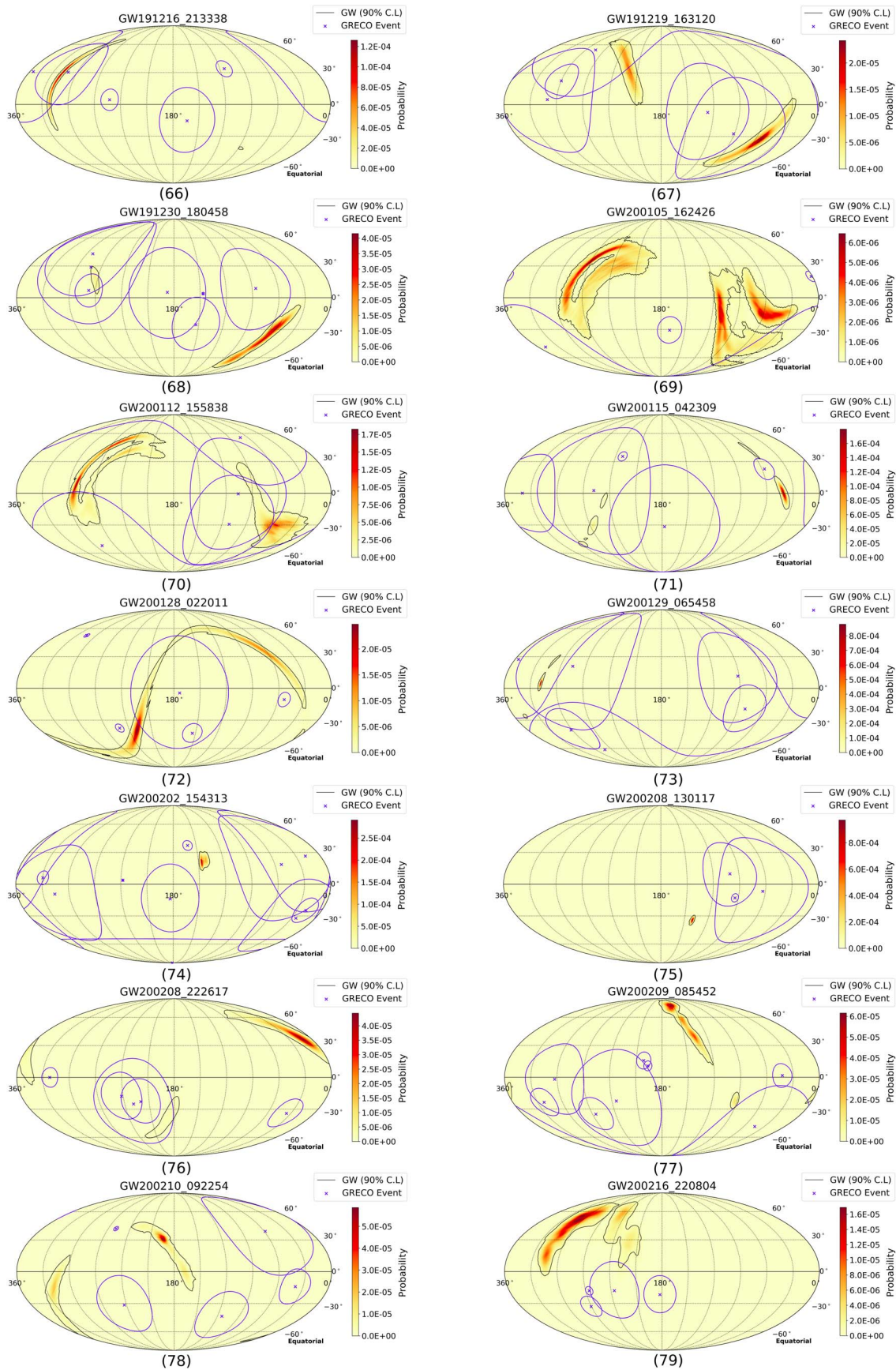
Figure 8. (Continued.)
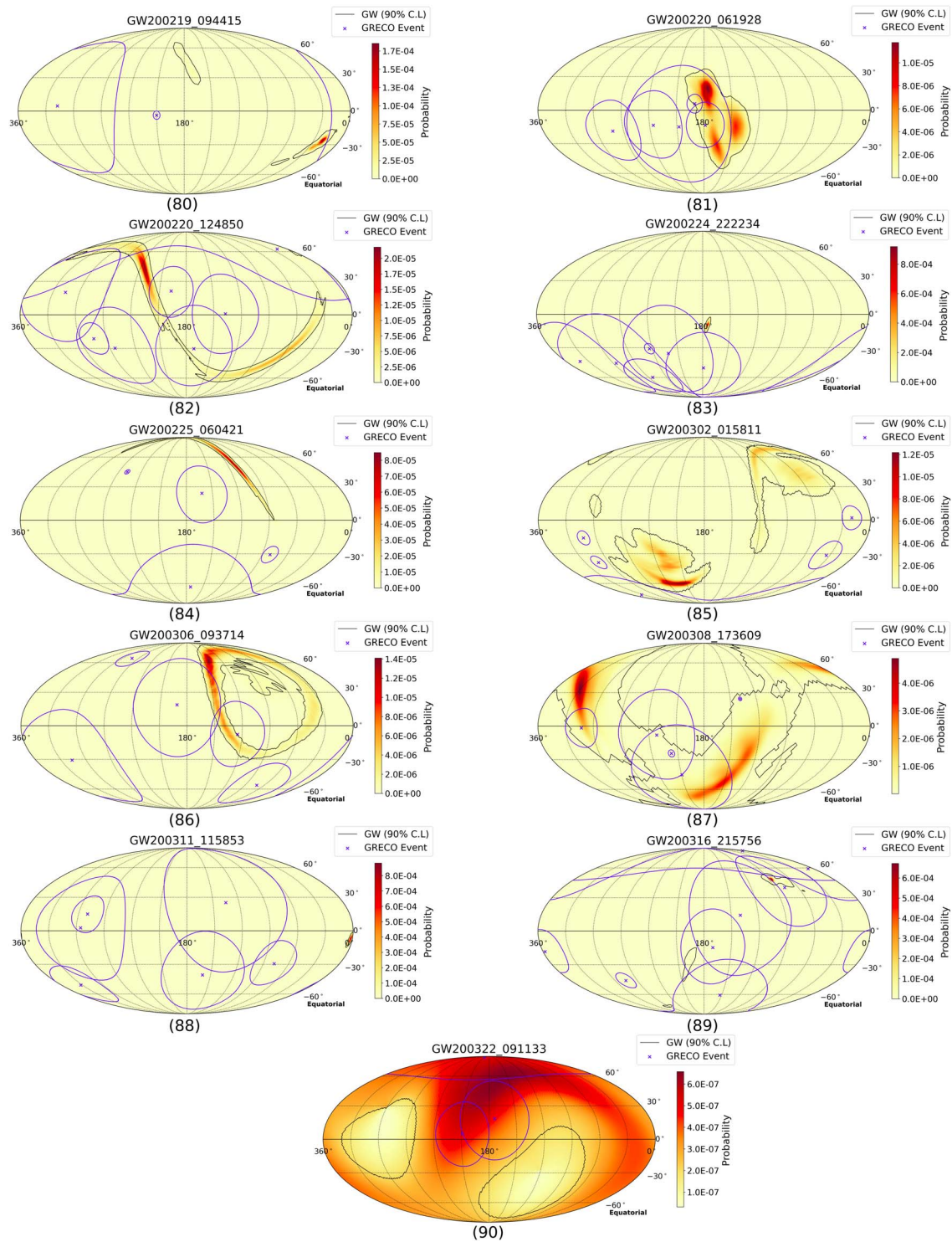
Figure 8. (Continued.)

ORCID iDs

R. Abbasi https://orcid.org/0000-0001-6141-4205
M. Ackermann https://orcid.org/0000-0001-8952-588X
S. K. Agarwalla https://orcid.org/0000-0002-9714-8866
J. A. Aguilar https://orcid.org/0000-0003-2252-9514
M. Ahlers https://orcid.org/0000-0003-0709-5631
J. M. Alameddine https://orcid.org/0000-0002-9534-9189
G. Anton https://orcid.org/0000-0003-2039-4724

C. Argüelles https://orcid.org/0000-0003-4186-4182
Y. Ashida https://orcid.org/0000-0003-4136-2086
S. N. Axani https://orcid.org/0000-0001-8866-3826
X. Bai https://orcid.org/0000-0002-1827-9121
A. Balagopal V. https://orcid.org/0000-0001-5367-8876
S. W. Barwick https://orcid.org/0000-0003-2050-6714
V. Basu https://orcid.org/0000-0002-9528-2009
J. J. Beatty https://orcid.org/0000-0003-0481-4952

J. Becker Tjus https://orcid.org/0000-0002-1748-7367
J. Beise https://orcid.org/0000-0002-7448-4189
C. Bellenghi https://orcid.org/0000-0001-8525-7515
S. BenZvi https://orcid.org/0000-0001-5537-4710
E. Bernardini https://orcid.org/0000-0003-3108-1141
D. Z. Besson https://orcid.org/0000-0001-6733-963X
E. Blaufuss https://orcid.org/0000-0001-5450-1757
S. Blot https://orcid.org/0000-0003-1089-3001
J. Y. Book https://orcid.org/0000-0001-6687-5959
C. Boscolo Meneguolo https://orcid.org/0000-0001-8325-4329
S. Böser https://orcid.org/0000-0002-5918-4890
O. Botner https://orcid.org/0000-0001-8588-7306
M. A. Campana https://orcid.org/0000-0003-4162-5739
C. Chen https://orcid.org/0000-0002-8139-4106
Z. Chen https://orcid.org/0000-0002-2813-7688
D. Chirkin https://orcid.org/0000-0003-4911-1345
B. A. Clark https://orcid.org/0000-0003-4089-2245
A. Coleman https://orcid.org/0000-0003-1510-1712
J. M. Conrad https://orcid.org/0000-0002-6393-0438
P. Coppin https://orcid.org/0000-0001-6869-1280
P. Correa https://orcid.org/0000-0002-1158-6735
D. F. Cowen https://orcid.org/0000-0003-4738-0787
P. Dave https://orcid.org/0000-0002-3879-5115
C. De Clercq https://orcid.org/0000-0001-5266-7059
J. J. DeLaunay https://orcid.org/0000-0001-5229-1995
D. Delgado López https://orcid.org/0000-0002-4306-8828
H. Dembinski https://orcid.org/0000-0003-3337-3850
A. Desai https://orcid.org/0000-0001-7405-9994
P. Desiati https://orcid.org/0000-0001-9768-1858
K. D. de Vries https://orcid.org/0000-0002-9842-4068
G. de Wasseige https://orcid.org/0000-0002-1010-5100
T. DeYoung https://orcid.org/0000-0003-4873-3783
A. Diaz https://orcid.org/0000-0001-7206-8336
J. C. Díaz-Vélez https://orcid.org/0000-0002-0087-0693
H. Dujmovic https://orcid.org/0000-0003-1891-0718
M. A. DuVernois https://orcid.org/0000-0002-2987-9691
P. Eller https://orcid.org/0000-0001-6354-5209
P. A. Evenson https://orcid.org/0000-0001-7929-810X
K. L. Fan https://orcid.org/0000-0002-8246-4751
K. Fang https://orcid.org/0000-0002-5387-8138
A. R. Fazely https://orcid.org/0000-0002-6907-8020
A. Fedynitch https://orcid.org/0000-0003-2837-3477
C. Finley https://orcid.org/0000-0003-3350-390X
D. Fox https://orcid.org/0000-0002-3714-672X
A. Franckowiak https://orcid.org/0000-0002-5605-2219
T. K. Gaisser https://orcid.org/0000-0003-4717-6620
E. Ganster https://orcid.org/0000-0003-4393-6944
A. Garcia https://orcid.org/0000-0002-8186-2459
A. Ghadimi https://orcid.org/0000-0002-6350-6485
C. Glaser https://orcid.org/0000-0001-5998-2553
T. Glauch https://orcid.org/0000-0003-1804-4055
T. Glüsenkamp https://orcid.org/0000-0002-2268-9297
S. Goswami https://orcid.org/0000-0002-0373-9770
S. J. Gray https://orcid.org/0000-0003-2907-8306
S. Griswold https://orcid.org/0000-0002-7321-7513
P. Gutjahr https://orcid.org/0000-0001-7980-7285
A. Hallgren https://orcid.org/0000-0001-7751-4489
L. Halve https://orcid.org/0000-0003-2237-6714
F. Halzen https://orcid.org/0000-0001-6224-2417
H. Hamdaoui https://orcid.org/0000-0001-5709-2100
A. Haungs https://orcid.org/0000-0002-9638-7574

K. Helbing https://orcid.org/0000-0003-2072-4172
F. Henningsen https://orcid.org/0000-0002-0680-6588
C. Hill https://orcid.org/0000-0003-0647-9174
W. Hou https://orcid.org/0000-0003-3422-7185
T. Huber https://orcid.org/0000-0002-6515-1673
K. Hultqvist https://orcid.org/0000-0003-0602-9472
G. S. Japaridze https://orcid.org/0000-0002-7000-5291
M. Jin https://orcid.org/0000-0003-0487-5595
B. J. P. Jones https://orcid.org/0000-0003-3400-8986
D. Kang https://orcid.org/0000-0002-5149-9767
W. Kang https://orcid.org/0000-0003-3980-3778
A. Kappes https://orcid.org/0000-0003-1315-3711
T. Karg https://orcid.org/0000-0003-3251-2126
M. Karl https://orcid.org/0000-0003-2475-8951
A. Karle https://orcid.org/0000-0001-9889-5161
U. Katz https://orcid.org/0000-0002-7063-4418
M. Kauer https://orcid.org/0000-0003-1830-9076
J. L. Kelley https://orcid.org/0000-0002-0846-4542
A. Khatee Zathul https://orcid.org/0000-0002-8735-8579
A. Kheirandish https://orcid.org/0000-0001-7074-0539
J. Kiryluk https://orcid.org/0000-0003-0264-3133
S. R. Klein https://orcid.org/0000-0003-2841-6553
A. Kochocki https://orcid.org/0000-0003-3782-0128
R. Koirala https://orcid.org/0000-0002-7735-7169
H. Kolanoski https://orcid.org/0000-0003-0435-2524
T. Kontrimas https://orcid.org/0000-0001-8530-6348
C. Kopper https://orcid.org/0000-0001-6288-7637
D. J. Koskinen https://orcid.org/0000-0002-0514-5917
P. Koundal https://orcid.org/0000-0002-5917-5230
M. Kovacevich https://orcid.org/0000-0002-5019-5745
M. Kowalski https://orcid.org/0000-0001-8594-8666
A. Kumar https://orcid.org/0000-0002-8367-8401
N. Kurahashi https://orcid.org/0000-0003-1047-8094
C. Lagunas Gualda https://orcid.org/0000-0002-9040-7191
M. Lamoureux https://orcid.org/0000-0002-8860-5826
M. J. Larson https://orcid.org/0000-0002-6996-1155
F. Lauber https://orcid.org/0000-0001-5648-5930
J. P. Lazar https://orcid.org/0000-0003-0928-5025
J. W. Lee https://orcid.org/0000-0001-5681-4941
K. Leonard DeHolton https://orcid.org/0000-0002-8795-0601
A. Leszczyńska https://orcid.org/0000-0003-0935-6313
Q. R. Liu https://orcid.org/0000-0003-3379-6423
E. Lohfink https://orcid.org/0000-0003-3248-5682
L. Lu https://orcid.org/0000-0003-3175-7770
F. Lucarelli https://orcid.org/0000-0002-9558-8788
A. Ludwig https://orcid.org/0000-0001-9038-4375
W. Luszczak https://orcid.org/0000-0003-3085-0674
Y. Lyu https://orcid.org/0000-0002-2333-4383
J. Madsen https://orcid.org/0000-0003-2415-9959
I. C. Mariş https://orcid.org/0000-0002-5771-1124
R. Maruyama https://orcid.org/0000-0003-2794-512X
F. McNally https://orcid.org/0000-0002-0785-2244
K. Meagher https://orcid.org/0000-0003-3967-1533
M. Meier https://orcid.org/0000-0002-9483-9450
S. Meighen-Berger https://orcid.org/0000-0001-6579-2000
L. Merten https://orcid.org/0000-0003-1332-9895
T. Montaruli https://orcid.org/0000-0001-5014-2152
R. W. Moore https://orcid.org/0000-0003-4160-4700
M. Moulai https://orcid.org/0000-0001-7909-5812
R. Naab https://orcid.org/0000-0003-2512-466X
R. Nagai https://orcid.org/0000-0001-7503-2777

J. Necker https://orcid.org/0000-0003-0280-7484
H. Niederhausen https://orcid.org/0000-0002-9566-4904
M. U. Nisa https://orcid.org/0000-0002-6859-3944
S. C. Nowicki https://orcid.org/0000-0003-2497-8057
A. Obertacke Pollmann https://orcid.org/0000-0002-2492-043X
B. Oeyen https://orcid.org/0000-0003-2940-3164
E. O'Sullivan https://orcid.org/0000-0003-1882-8802
H. Pandya https://orcid.org/0000-0002-6138-4808
N. Park https://orcid.org/0000-0002-4282-736X
E. N. Paudel https://orcid.org/0000-0001-9276-7994
C. Pérez de los Heros https://orcid.org/0000-0002-2084-5866
J. Peterson https://orcid.org/0000-0002-7985-1443
S. Philippen https://orcid.org/0000-0002-0276-0092
A. Pizzuto https://orcid.org/0000-0002-8466-8168
M. Plum https://orcid.org/0000-0001-8691-242X
B. Pries https://orcid.org/0000-0003-4811-9863
A. Rehman https://orcid.org/0000-0001-7616-5790
P. Reichherzer https://orcid.org/0000-0003-4513-8241
E. Resconi https://orcid.org/0000-0003-0705-2770
S. Reusch https://orcid.org/0000-0002-7788-628X
W. Rhode https://orcid.org/0000-0003-2636-5000
B. Riedel https://orcid.org/0000-0002-9524-8943
M. Rongen https://orcid.org/0000-0002-7057-1007
C. Rott https://orcid.org/0000-0002-6958-6033
D. Ryckbosch https://orcid.org/0000-0002-8759-7553
I. Safa https://orcid.org/0000-0001-8737-6825
D. Salazar-Gallegos https://orcid.org/0000-0002-9312-9684
A. Sandrock https://orcid.org/0000-0002-6779-1172
M. Santander https://orcid.org/0000-0001-7297-8217
S. Sarkar https://orcid.org/0000-0002-1206-4330
S. Sarkar https://orcid.org/0000-0002-3542-858X
H. Schieler https://orcid.org/0000-0002-2637-4778
S. Schindler https://orcid.org/0000-0001-5507-8890
F. Schlüter https://orcid.org/0000-0002-5545-4363
J. Schneider https://orcid.org/0000-0001-7752-5700
F. G. Schröder https://orcid.org/0000-0001-8495-7210
L. Schumacher https://orcid.org/0000-0001-8945-6722
S. Sclafani https://orcid.org/0000-0001-9446-1219
S. Seunarine https://orcid.org/0000-0003-3272-6896
A. Sharma https://orcid.org/0000-0001-5397-6777
M. Silva https://orcid.org/0000-0001-6940-8184
B. Smithers https://orcid.org/0000-0003-1273-985X
J. Soedingrekso https://orcid.org/0000-0003-1011-2797
D. Soldin https://orcid.org/0000-0003-3005-7879
G. Sommani https://orcid.org/0000-0002-0094-826X
G. M. Spiczak https://orcid.org/0000-0002-0030-0519
C. Spiering https://orcid.org/0000-0001-7372-0074
T. Stezelberger https://orcid.org/0000-0003-2676-9574
T. Stuttard https://orcid.org/0000-0001-7944-279X
G. W. Sullivan https://orcid.org/0000-0002-2585-2352
I. Taboada https://orcid.org/0000-0003-3509-3457
S. Ter-Antonyan https://orcid.org/0000-0002-5788-1369
W. G. Thompson https://orcid.org/0000-0003-2988-7998
K. Tollefson https://orcid.org/0000-0001-9725-1479
S. Toscano https://orcid.org/0000-0002-1860-2240
A. Trettin https://orcid.org/0000-0003-0350-3597
C. F. Tung https://orcid.org/0000-0001-6920-7841
M. A. Unland Elorrieta https://orcid.org/0000-0002-6124-3255
N. Valtonen-Mattila https://orcid.org/0000-0002-1830-098X

J. Vandenbroucke https://orcid.org/0000-0002-9867-6548
N. van Eijndhoven https://orcid.org/0000-0001-5558-3328
J. van Santen https://orcid.org/0000-0002-2412-9728
S. Verpoest https://orcid.org/0000-0002-3031-3206
C. Walck https://orcid.org/0000-0002-4188-9219
T. B. Watson https://orcid.org/0000-0002-8631-2253
C. Weaver https://orcid.org/0000-0003-2385-2559
J. Weldert https://orcid.org/0000-0002-3709-2354
C. Wendt https://orcid.org/0000-0001-8076-8877
N. Whitehorn https://orcid.org/0000-0002-3157-0407
C. H. Wiebusch https://orcid.org/0000-0002-6418-3008
M. Wolf https://orcid.org/0000-0001-9991-3923
S. Yoshida https://orcid.org/0000-0003-2480-5105
T. Yuan https://orcid.org/0000-0002-7041-5872
Z. Zhang https://orcid.org/0000-0002-7347-283X

References

Aartsen, M. G., Ackermann, M., Adams, J., et al. 2017, JInst, 12, P03012
Aartsen, M. G., Ackermann, M., Adams, J., et al. 2018, Sci, 361, eaat1378
Aartsen, M. G., Ackermann, M., Adams, J., et al. 2020, ApJL, 898, L10
Abbasi, R., Ackermann, M., Adams, J., et al. 2021, arXiv:2105.13160
Abbasi, R., Ackermann, M., Adams, J., et al. 2023b, ApJ, 953, 160
Abbasi, R., Ackermann, M., Adams, J., et al. 2022, Sci, 378, 538
Abbasi, R., Ackermann, M., Adams, J., et al. 2023a, ApJ, 944, 80
Abbasi, R., et al. 2012, APh, 35, 615
Abbott, B. P., Abbott, R., Abbott, T. D., et al. 2017, ApJL, 848, L13
Abbott, B. P., Abbott, R., Abbott, T. D., et al. 2019, PhRvX, 9, 031040
Abbott, B. P., Abbott, R., Abbott, T. D., et al. 2020, ApJL, 892, L3
Abbott, R., Abbott, T. D., Abraham, S., et al. 2021a, PhRvX, 11, 021053
Abbott, R., Abbott, T. D., Acernese, F., et al. 2021b, arXiv:2108.01045
Abbott, R., Abbott, T. D., Acernese, F., et al. 2021c, PhRvX, 11, 021053
Abe, K., Bronner, C., Hayato, Y., et al. 2021, ApJ, 918, 78
Abe, S., Asami, S., Gando, A., et al. 2021, ApJ, 909, 116
Acernese, F., Agathos, M., Agatsuma, K., et al. 2015, CQGra, 32, 024001
Agostini, M., Altenmüller, K., Appel, S., et al. 2020, ApJ, 850, 21
Ahlers, M., & Halser, L. 2019, MNRAS, 490, 4935
Albert, A., André, M., Anghinolfi, M., et al. 2017, ApJL, 850, L35
Albert, A., André, M., Anghinolfi, M., et al. 2020, EPJC, 80, 487
Alexander, K. D., Berger, E., Fong, W., et al. 2017, ApJL, 848, L21
Balagopal, V. A., Hussain, R., Pizzuto, A., et al. 2021, in 37th ICRC 2021 (Trieste: SISSA), 39
Baret, B., Bartos, I., Bouhou, B., et al. 2011, APh, 35, 1
Bartos, I., Beloborodov, A. M., Hurley, K., & Márka, S. 2013, PhRvL, 110, 241101
Biehl, D., Heinze, J., & Winter, W. 2018, MNRAS, 476, 1191
Carpio, J. A., & Murase, K. 2020, PhRvD, 101, 123002
Coulter, D. A., Foley, R. J., Kilpatrick, C. D., et al. 2017, Sci, 358, 1556
Fang, K., & Metzger, B. D. 2017, ApJ, 849, 153
Górski, K. M., Hivon, E., Banday, A. J., et al. 2005, ApJ, 622, 759
Gottlieb, O., & Globus, N. 2021, ApJL, 915, L4
Hallinan, G., Corsi, A., Mooley, K. P., et al. 2017, Sci, 358, 1579
IceCube Collaboration, Aartsen, M. G., Abraham, K., et al. 2016, JInst, 11, P11009
IceCube Collaboration, Aartsen, M. G., Ackermann, M., et al. 2018, Sci, 361, 147
Kintscher, T. & IceCube Collaboration 2016, JPhCS, 718, 062029
LIGO Scientific Collaboration, Aasi, J., Abbott, B. P., et al. 2015, CQGra, 32, 074001
LIGO Scientific Collaboration, Virgo Collaboration 2019, GWTC-1 Data Release, www.gw-openscience.org/GWTC-1/
LIGO Scientific Collaboration, Virgo Collaboration 2021, GWTC-2.1 Data Release, www.gw-openscience.org/GWTC-2.1/
LIGO Scientific Collaboration, Virgo Collaboration, KAGRA Collaboration 2021, GWTC-3 Data Release, www.gw-openscience.org/GWTC-3/
Murase, K., & Bartos, I. 2019, ARNPS, 69, 477
Murase, K., Kashiyama, K., & Mészáros, P. 2013, PhRvL, 111, 131102
Smartt, S. J., Chen, T. W., Jerkstrand, A., et al. 2017, Natur, 551, 75
Troja, E., Piro, L., van Eerten, H., et al. 2017, Natur, 551, 71
Veske, D., IceCube, Abbasi, R., et al. 2021, in 37th ICRC (Trieste: SISSA), 950